Master thesis and internship[BR]- Master's thesis : Cartesian high order solver for plasma flows[BR]- Integration Internship

Auteur : Soave, Alessandro
Promoteur(s) : Hillewaert, Koen
Faculté : Faculté des Sciences appliquées
Diplôme : Master en ingénieur civil en aérospatiale, à finalité spécialisée en "aerospace engineering"
Année académique : 2021-2022
URI/URL : http://hdl.handle.net/2268.2/16430

Faculté des Sciences appliquées

Cartesian high order solver applied to plasma flows

Master's thesis carried out to obtain the degree of Master of Science in Aerospace Engineering

Author: Soave Alessandro

Advisors: Hillewaert Koen
Magin Thierry

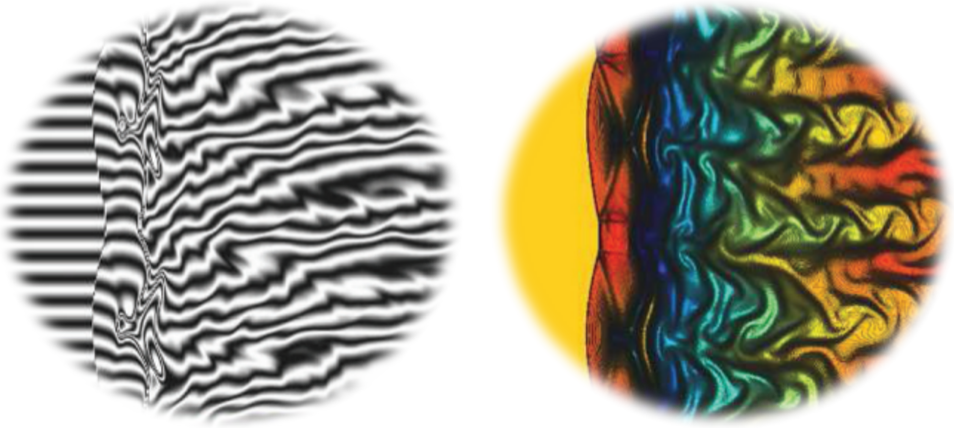

Academic year 2021 - 2022

Acknowledgements

J'aimerais tout d'abord remercier ma famille, mes parents et mes amis proches qui ont toujours été à mes côtés et mon soutenu non seulement pour ce projet mais tout au long de mes études.

J'aimerais aussi remercier Giuseppe Gangemi pour m'avoir prêté son aide et m'avoir accompagné dans cette épreuve, Nicolas Corthouts pour ses conseils avisés mais aussi pour m'avoir accueilli dans son beau bureau à l'Université de Liège, ainsi que Nayan Levaux, Amaury Bilocq et à toute l'équipe FORDGE.

Enfin, j'aimerais porter un grand remerciement à mes promoteurs, Koen Hillewaert et Thierry Magin pour m'avoir soutenu et guidé tout au long de mon travail. Sans doute leurs expertises respectives ainsi que leur bienveillance m'ont été d'une aide inestimable.

I would like to begin by thanking my family, parents and close friends who have always been by my side and supported me not only in this project but throughout my academic journey.

I would also like to thank Giuseppe Gangemi for his help and his support in this challenging task, Nicolas Corthouts for his wise advices but also for welcoming me in his beautiful office at the *Université de Liège*, as well as Nayan Levaux, Amaury Bilocq and the whole FORDGE team.

Finally, I would like to specially thank my supervisors, Koen Hillewaert and Thierry Magin for having supported me and guided me throughout my work. Undoubtedly their respective expertise as well as their kindness and understanding has been invaluable to me.

Contents

Introduction

In the past decades, the study of plasma flows has gain significant importance in scientific research. Indeed, many applications have resulted from it. From day to day applications, such as screen technologies with PDP (plasma display panels) [8], manufacturing applications or even more recently medical application [36], to high end promising technologies such as the Tokamak fusion reactor [11, 12] or the Hall thruster electric drive [1, 9, 10, 15, 24, 33]. This last application is of particular interesting in the field of CFD as the physics of it can display various challenges and are still somewhat misunderstood.

In brief, the Hall thruster works by using an electrostatic potential to accelerate ions to high speeds, ejecting them and thus produce thrust. Typically, the Hall thruster uses a Xenon gas, the ion being positively charged charge. Contrary to grid thruster, the Hall thruster differs as no grid is present, instead the negative charge used to attract positve ions is provided by electrons which are injected from the end of the thruster.
The thruster is composed of two concentric radial magnets inducing then a radial magnetic field in between the two magnets. Under such field a circular motion is induced on charged particles. The radius of such motion is in effect depended on the mass and strength of the field. The field is then calibrated to only be able to deflect electrons capturing electrons and cause a disparity between the density of ions and electrons. The result is the creation of an electric field. Moreover, the ions tend to drift in the axial direction of the thruster, thus an axial electric field appears. The electric field contributes in the acceleration of charged particles toward the end of the thruster.
Xenon is then fed from the back of the thruster by collision with the confined electrons, the gas is ionized, creating more charged particles in which ions will be accelerate towards the exhaust and electrons will be confined in the thruster. This cycle can be stabilised given that a steady flow of Xenon and electrons is fed in the chamber. Indeed, ions exiting the thruster will pull a portion of the confined electrons. This pulling is what causes the characteristic blue plume of the thruster. A schematic of the process described is shown in Fig. 1.

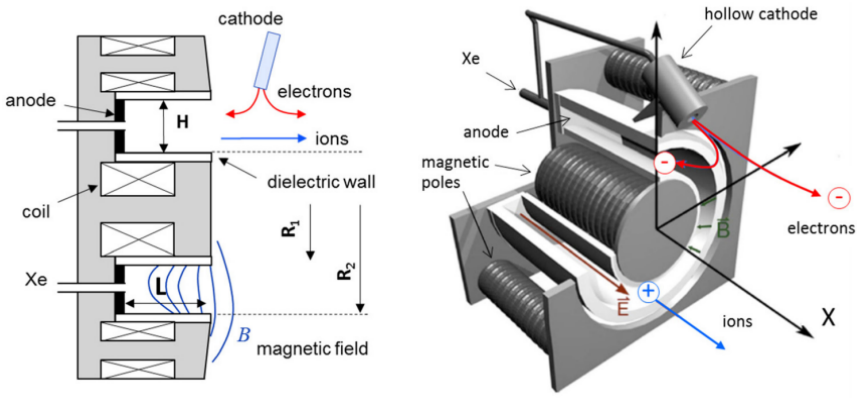

Figure 1: Diagram of the Hall thruster from [9]

As mentioned previously, the simulation of the plasma flow inside such device is an ongoing field of research in CFD. Particularly, the Hall thruster introduces several challenging aspect. On one hand, the simulation needs to capture electric and magnetic field interactions with the plasma flow. On the other, the solver should also be able to capture chemical interaction between reacting species (either by collisional or radiative mechanisms). Furthermore, the characteristic times associated to chemical reactions and the fluid motion tend to differ in magnitude (the chemistry being much faster). Lastly, plasma simulations, regardless of the application, are particularly challenging as the strong disparity in mass between electron and atomic species (also referred as heavy species) implies then very stiff problems.

Such research is for instance currently being done at the *Université de Liège* by professor K. Hillewaert and his students. This work inscribes itself in the continuation of the previous research in which methodologies to tackle interactions between the electric field and the plasma flow have been successfully developed in the works of N. Corthouts [17] and F. Custinne [18]. For this work, the focus will be on a different aspect of the overall problematic. The focus is on the chemistry, the goal is then to develop a methodology to resolve reactive plasama flows.

To do so, a post-shock relaxation problem is considered. Such problem incorporates several challenging aspect relevant to the Hall thruster research. The problem at hand was introduced in [46] and many have then studied the numerical resolution of such problems [4, 7, 31, 32]. In particular, this works refers to the work of Kapper [31, 32] which has solved this problem in the one and two dimensional case using for a State-to-State chemical model.

The present work is then split in three parts: the physics of the studied plasma, the numerical methodology of this work and lastly the results with the previous considerations.
In the first part, the governing equations are established with a Multi-fluid formulation [4, 35]. Then the chemistry of the studied plasma is presented. Moreover, this part introduces models for the chemical behaviour of the plasma based on literature [5, 6, 14, 35, 42, 43, 45, 49]. Lastly, the problem of interest of this work is defined.
In the second part, the discretisation of the governing equations is done following a Discontinuous Galerkin Finite Element Method (DG-FEM). Additionally, schemes to solve the system of equations are presented for steady and unsteady simulations.
Finally, the last part of this work presents the results up to date of the problem obtained with the DG-FEM formulation. A final discussion is done in order to assess the successes or the failures of particular points in the overall methodology presented in this work.

Part I

Plasma physics

Chapter 1

Governing equations

In this chapter, the governing equations for a quasi-neutral plasma mixture are developed. To do so, the following methodology is taken. First the micro scale behaviour of the system is described using a probabilistic approach. Such method is often employed to describe gas dynamics but remains valid for plasma flows. The difference for the latter is that additional effects on the flow need to be considered such as the influence of electromagnetic fields and ionization mechanisms. From the micro scale description of the flow, the macroscopic behaviour of the system is obtained by considering a Multi-fluid formulation.

Before diving into each approach, note that the developments presented here follow the methodology presented in [5, 42, 43], the derivations are then restricted to the relevant aspects of this work.

1.1 Statistical approach

Similar to gases, a plasma can be described from a statistical point of view as a mixture of charged particle. Such approach is sometimes also called a kinetic description, as the statistical aspect of it relates to the variation in velocity of the particles composing the plasma (or gas in general) with respect to the overall mixture velocity. Considering that gases are composed of a significant number of particles, one can understand how a statistical approach is often privileged when describing gas dynamics (rather than describing each particle's behaviour).

Contrary to gases a plasma is by definition multi-species. To denote its composition, the $\mathcal{S}$ notation is introduced referring to the set of species composing the plasma mixture. Note that this notation will remain for the rest of this work. The particle density of a given species α in the mixture follows then a certain distribution f_α, itself function of the particle's velocity $\boldsymbol{v}_\alpha$, its position $\boldsymbol{x}$ and time t. The conservation of f_α for a moving fluid is then described with the Boltzmann equation [42],

$$\partial_t f_\alpha + \boldsymbol{v}_\alpha \cdot \nabla f_\alpha + \nabla_{\boldsymbol{v}_\alpha} \cdot \left(f_\alpha \frac{\boldsymbol{F}_\alpha}{m_\alpha} \right) = \sum_{\beta \in \mathcal{S}} J_{\alpha\beta} + \Gamma_\alpha \tag{1.1}$$

where $\boldsymbol{F}_\alpha$ is the total force acting on the particle, $J_{\alpha\beta}$ accounting for elastic interactions with other particles in the plasma mixture $\mathcal{S}$ and Γ_α accounting for the production of particles α from ionization processes. Furthermore, the total force is the resultant force of the electric and magnetic fields acting on particle α. In this work, no such effects will be considered and the focus is then shifted on the sources in Eq. (1.1). The Boltzmann equation is the basis for the Multi-fluid model as considering f_α for higher moments gives then a system of equations

describing the conservation of mass, momentum and total energy of the system at a macro scale.

1.2 The Multi-fluid model

Let's now obtain the governing equation for local macro scale quantities. The derivation of the Multi-fluid model equations is well documented in literature, here the derivation follows the methodology presented in [5, 43].

The macro scale quantities of interest are defined by integrating the distribution function f_α over the velocity space, one can then define for a given species α the particle density n_α, the mean velocity $\mathbf{v}_\alpha$ and the internal energy $\mathcal{U}_\alpha$ as follows.

$$n_\alpha(\boldsymbol{x}, t) = \int_{\mathbb{R}^3} f_\alpha\left(\boldsymbol{x}, \boldsymbol{v}_\alpha, t\right) d\boldsymbol{v}_\alpha \tag{1.2}$$

$$\mathbf{v}_\alpha(\boldsymbol{x}, t) = \langle \boldsymbol{v}_\alpha(\boldsymbol{x}, t) \rangle = \frac{1}{n_\alpha(\boldsymbol{x}, t)} \int_{\mathbb{R}^3} \boldsymbol{v}_\alpha \, f_\alpha\left(\boldsymbol{x}, \boldsymbol{v}_\alpha, t\right) d\boldsymbol{v}_\alpha \tag{1.3}$$

$$\mathcal{U}_\alpha(\boldsymbol{x}, t) = \frac{1}{n_\alpha(\boldsymbol{x}, t)} \int_{\mathbb{R}^3} \frac{1}{2} \left(\boldsymbol{v}_\alpha - \mathbf{v}_\alpha\right)^2 f_\alpha\left(\boldsymbol{x}, \boldsymbol{v}_\alpha, t\right) d\boldsymbol{v}_\alpha \tag{1.4}$$

Similarly, one can describe the evolution of such quantities by multiplying f_α by a collision invariant ψ_α, injecting it back in the Boltzmann equation (1.1) and averaging over the velocity space. Choosing the collision invariants 1, $\boldsymbol{v}_\alpha$ and $\boldsymbol{v}_\alpha \cdot \boldsymbol{v}_\alpha/2$ gives then a set of conservation equations for particle density, momentum and total energy. Additionally, the plasma is assumed to be isotropic. One implication is for instance that the particle mass of species α is constant in time and space, $m_\alpha\left(\boldsymbol{x}, t\right) = m_\alpha$. This in turn means that the conservation equation for particle density is equivalent to the conservation equation for mass, also known as continuity equation for fluids.

$$\rho_\alpha(\boldsymbol{x}, t) = m_\alpha n_\alpha(\boldsymbol{x}, t) \tag{1.5}$$

The conservation equation, irrespective of which invariant is chosen, is the following,

$$\begin{aligned} \partial_t \left(n_\alpha \langle \psi_\alpha \rangle \right) + \nabla \cdot \left(n_\alpha \langle \psi_\alpha \boldsymbol{v}_\alpha \rangle \right) - n_\alpha \left(\langle \partial_t \psi_\alpha \rangle + \langle \boldsymbol{v}_\alpha \cdot \nabla \psi_\alpha \rangle \right) = \sum_{\beta \in \mathcal{S}} \int_{\mathbb{R}^3} \psi_\alpha J_{\alpha\beta} d\boldsymbol{v}_\alpha \\ + \int_{\mathbb{R}^3} \psi_\alpha \Gamma_\alpha d\boldsymbol{v}_\alpha \end{aligned} \tag{1.6}$$

where the average operator of the collision invariant ψ_α is defined as

$$n_\alpha \langle \psi_\alpha \rangle = \int_{\mathbb{R}^3} \psi_\alpha f_\alpha d\boldsymbol{v}_\alpha.$$

Before developing each equation, it is important to introduce some key properties of the average operator $\langle . \rangle$ for isotropic fluids.

It is common practice in fluid mechanics to express the velocity of the fluid into a sum of an average velocity $\mathbf{v}$ and a perturbation velocity $\boldsymbol{v}'$. The fluid has then the following properties :

- The average of the perturbation velocity is zero.

$$\langle \boldsymbol{v} \rangle = \langle \mathbf{v} \rangle + \langle \boldsymbol{v}' \rangle = \mathbf{v}$$

- The average of the squared perturbation velocity is non zero for same direction products.

$$\left\langle v_i' v_j' \right\rangle = 0 \,, \text{ if } \; i \neq j$$

- The average of the terms $\langle \partial_t \psi \rangle$ and $\langle \boldsymbol{v} \cdot \nabla \psi \rangle$ are zero with the considered invariants [35, 43, 49].

Furthermore, the temperature of species α at a macroscopic scale can be derived from microscopic kinetic relation as expressed in Boltzmann theory of gases giving us then an expression for $\langle v_i' v_i' \rangle$,

$$\frac{m_\alpha \left\langle v_i'^2 \right\rangle}{2} = \frac{k_B \, T_\alpha}{2}$$

where k_B is the Boltzman constant. The average of the square velocity can be then fully expressed in each directions.

$$\begin{aligned}
\langle v_i v_j \rangle &= \left\langle \left(\mathrm{v}_i + v_i' \right) \left(\mathrm{v}_j + v_j' \right) \right\rangle \\
&= \langle \mathrm{v}_i \mathrm{v}_j \rangle + \left\langle v_i' v_j' \right\rangle + \mathrm{v}_i \left\langle v_j' \right\rangle + \mathrm{v}_j \left\langle v_i' \right\rangle \\
&= \mathrm{v}_i \mathrm{v}_j + \left\langle v_i' v_j' \right\rangle \\
&= \mathrm{v}_i \mathrm{v}_j + \delta_{ij} \frac{k_B \, T_\alpha}{m_\alpha}
\end{aligned}$$

Additionnally, each fluid is assumed to behave as a perfect gas, therefore the expression obtained just above is equivalent to

$$n_\alpha \langle v_i v_j \rangle = n_\alpha \mathrm{v}_i \mathrm{v}_j + \delta_{ij} \frac{p_\alpha}{m_\alpha} \tag{1.7}$$

where $p_\alpha = n_\alpha k_B T_\alpha$ is the pressure of species α. Moreover, from the perfect gas assumption, the total energy per unit mass E_α and the enthalpy H_α of species α can be defined in relation to the previous quantities.

$$E_\alpha = \mathcal{U}_\alpha + \frac{1}{2} \left(\mathbf{v}_\alpha \cdot \mathbf{v}_\alpha \right) \tag{1.8}$$

$$H_\alpha = E_\alpha + \frac{p_\alpha}{\rho_\alpha} \tag{1.9}$$

Finally, returning back to Eq. (1.6) and developing each equation with the chosen invariant, neglecting the stress tensor terms and considering only the one dimensional case, the governing equations for the studied plasma flow of the present work are :

$$\partial_t n_\alpha + \partial_x \left(n_\alpha u_\alpha \right) = S_\alpha^{(n)} \tag{1.10}$$

$$\partial_t \left(n_\alpha u_\alpha \right) + \partial_x \left(n_\alpha u_\alpha^2 + \frac{p_\alpha}{m_\alpha} \right) = S_\alpha^{(m)} \tag{1.11}$$

$$\partial_t \left(n_\alpha E_\alpha \right) + \partial_x \left(n_\alpha H_\alpha u_\alpha \right) = -\frac{1}{m_\alpha} \partial_x q_\alpha + S_\alpha^{(e)} \tag{1.12}$$

where m_α, n_α, u_α, E_α, p_α and q_α are respectively the mass, the particle density, the mean velocity in the x direction, the total energy per unit mass, the static pressure and the heat flux associated to particle α. The terms $S_\alpha^{(n)}$, $S_\alpha^{(m)}$ and $S_\alpha^{(e)}$ are the source terms and refer respectively to the production of particle density, momentum and total energy. The source terms can be further split into a contribution from elastic collisions and a contribution from inelastic collisions. In this case, inelastic collision are understood as chemical reaction due to collision between reacting species. The source term can be generalized for each equation as

$$S_\alpha^{(k)} = \frac{1}{m_\alpha} \sum_{\beta \in \mathcal{S}} r_{\alpha\beta}^{(k)} + \dot{\omega}^{(k)} \tag{1.13}$$

where the k superscipt refer to a given equation in the system of Eqs. (1.10–1.12), $r_{\alpha\beta}^{(k)}$ and $\dot{\omega}^{(k)}$ are respectively the exchange of the given conserved quantity between particle of species α and particle of species β due to elastic collisions and the production of the conserved quantity for species α due to the underlying chemical processes. The modeling of these terms will be further developed in the next chapter.
Furthermore, the heat flux q_α is modeled with the Fourier law as no radiative processes are considered in this work. The heat conductivity κ_α of species α will also be detailled in the next chapter.

$$q_\alpha = -\kappa_\alpha \partial_x T_\alpha \tag{1.14}$$

Before ending this chapter, it is also useful to define so called state function relating important thermodynamical quantities such as temperature and pressure to the conserved variables. One can then fully describe the evolution of the system from a thermodynamical point of view with the system of Eqs. (1.10)–(1.12) previously defined. Let us then introduce the vector of conserved variables for a given species α :

$$\boldsymbol{U}_\alpha = \begin{bmatrix} n_\alpha & n_\alpha u_\alpha & n_\alpha E_\alpha \end{bmatrix}^\mathsf{T},$$

the pressure state function is found with the perfect gas relation relating internal energy to pressure.

$$\frac{p_\alpha}{m_\alpha} = (\gamma_\alpha - 1)\left(U_{\alpha,3} - \frac{1}{2}\frac{U_{\alpha,2}^2}{U_{\alpha,1}}\right) \tag{1.15}$$

Here γ_α is the heat capacity ratio of species α. Furthermore, one can relate pressure to temperature, enthalpy and speed of sound.

$$T_\alpha = (\gamma_\alpha - 1)\frac{m_\alpha}{k_B}\left(\frac{U_{\alpha,3}}{U_{\alpha,1}} - \frac{1}{2}\frac{U_{\alpha,2}^2}{U_{\alpha,1}^2}\right) \tag{1.16}$$

$$H_\alpha = \gamma_\alpha \frac{U_{\alpha,3}}{U_{\alpha,1}} - \frac{1}{2}(\gamma_\alpha - 1)\frac{U_{\alpha,2}^2}{U_{\alpha,1}^2} \tag{1.17}$$

$$c_\alpha = \sqrt{\gamma_\alpha \frac{p_\alpha}{\rho_\alpha}} = \sqrt{\gamma_\alpha(\gamma_\alpha - 1)\left(\frac{U_{\alpha,3}}{U_{\alpha,1}} - \frac{1}{2}\frac{U_{\alpha,2}^2}{U_{\alpha,1}^2}\right)} \tag{1.18}$$

Chapter 2

Chemistry and source modeling

In the previous chapter, the general form of the system of equations for the studied plasma flow was derived but some terms were not fully defined. These terms are linked to the chemistry of the plasma and should be modeled accordingly. The goal of this chapter is then to describe the considered chemistry of the plasma and provide a description for the undefined terms in Eqs. (1.10–1.12), i.e the source terms and the heat conductivity.

In the context of this work, an argon plasma is considered. The specification of the plasma are first described following a multi-temperature model (MT). Then from the model, the inelastic and elastic contribution to the source terms are described. Lastly, important parameters linked to the chemical properties of the plasma are defined such as the heat conductivity or the inter- and intra-species collision frequencies.

Furthermore, to aid in the computation of chemical interactions within the plasma, the MUTATION^{++} library is used. MUTATION^{++} is an open-source library developed at the von Karman Institute for Fluid Dynamics (VKI) with the goal to assist particular CFD application by providing a robust interface to compute transport, thermodynamical and chemical properties of the fluid. Such application are for instance, hypersonic flows or plasma flows. A full description of its implementation and functioning is available in [45]. Note that the practical uses of MUTATION^{++} for this work will later be detailed in Chapter 5.

2.1 The Argon 3 multi-temperature model

The Argon 3 plasma model is composed of three species following a MT approach. The set of pseudo-species of the plasma is then composed of a single neutral, one ion and an electron. The set will be referred then as $\mathcal{S}_3 = \left\{\mathrm{e}^-, \mathrm{Ar}, \mathrm{Ar}^+\right\}$. Furthermore, the atom species are supposed to be at their groundstate. The chemical reaction are then only collisional in nature, two reactions are considered and are denoted from their forward mechanism: an atom-electron impact ionization and an atom-atom impact ionization process. Note that the backward mechanism can be seen as recombination processes.

$$\mathrm{Ar} + \mathrm{e}^- \rightleftharpoons \mathrm{Ar}^+ + 2\mathrm{e}^- \tag{2.1}$$

$$\mathrm{Ar} + \mathrm{Ar} \rightleftharpoons \mathrm{Ar} + \mathrm{Ar}^+ + \mathrm{e}^- \tag{2.2}$$

From here, the production of a given species is computed from the Law of mass action as described in [45], which states that the rate of production of a reaction is proportional to the rate of progress $\mathfrak{R}$ of the reaction. The rate of progress is defined as the difference between the product of the reactant concentrations raised to the forward stoichiometry coefficients and the

product concentrations raised to the backward coefficents. For example, the rate of progress of Eq. (2.1) is

$$\mathfrak{R} = k_f \left[\mathrm{Ar}\right] \left[\mathrm{e}^-\right] - k_b \left[\mathrm{Ar}^+\right] \left[\mathrm{e}^-\right]^2 \tag{2.3}$$

where k_f and k_b are respectively the forward and backward rate coefficients, independent from the species concentrations. The production rate of each species is then proportional to Eq. (2.3).

$$\dot{\omega} \propto k_f \left[\mathrm{Ar}\right] \left[\mathrm{e}^-\right] - k_b \left[\mathrm{Ar}^+\right] \left[\mathrm{e}^-\right]^2 \tag{2.4}$$

To generalize, the forward and backward stoichiometry coefficients will be referred with the ν' and ν'' notation respectively.

As shown in the previous equations, the rate coefficients are key parameters in the computation of the production rates. In practice, the rate coefficient are dependent on the collision frequency between the reactants but also if the collisions has enough energy to trigger the reaction. In many applications, these rates are modeled by the modified Arrhenius rate law

$$k\left(T\right) = A\, T^n\, e^{-\frac{T_a}{T}} \tag{2.5}$$

where k is function of the temperature T and A, n and T_a are constants determining the behaviour of the Arrhenius law. The exponent term n in Eq. (2.5) models the dependency of the collision frequency to the temperature while the exponential term acts as an activation function where T_a is the activation temperature for a given reaction. The constant A can be seen as an intensity factor. Furthermore, to distinguish between forward and backward, it is often common practice to compute the forward coefficient from the Arrhenius rate law while the backward coefficient is evaluated from the equilibrium constant at a temperature linked to the backward reaction mechanism.

$$k_b\left(T_b\right) = \frac{k_f^{eq}\left(T_b\right)}{K_{eq}\left(T_b\right)} \tag{2.6}$$

However, the backward coefficient can also be modeled from the Arrhenius rate law and thus follows the same expression of Eq. (2.5) but evolving at the backward reaction temperature with different Arrhenius parameter values. This approach is preferred for this work.

$$k_f\left(T_f\right) = A\, T_f^n\, e^{-\frac{T_a}{T_f}} \tag{2.7}$$

$$k_b\left(T_b\right) = A\, T_b^n\, e^{-\frac{T_a}{T_b}} \tag{2.8}$$

The coefficient of the Arrhenius law have been derived in [2] for the atom-electron reaction. The forward parameters for the atom-atom reaction are taken from [7]. While the backward atom-atom Arrhenius parameters have been determined by retrofitting the backward coefficient curve for different regimes of temperature with the MUTATION^{++} library. The parameters are summarised in Table. 2.1 for the forward coefficients and Table. 2.2 for the backward coefficients. However, some incoherence was observed regarding the units of the constants A in the Arrhenius law. Indeed, it is common practice to express A in terms of $\mathrm{m^3mol^{-1}s^{-1}}$ regardless of the stoichiometry coefficients and the exponent n. This is not consistent, one can show in Eq. (2.3) that the units of k (being a generic rate coefficient) should be $\mathrm{m^3mol^{-N}s^{-1}}$, where N here is the number of reacting species for the considered reaction. Therefore, to fix this inconsistency, the units of A are not indicated in Table. 2.1 and Table. 2.2, one should then assume that the value displayed has the appropriate units, i.e units that ensure the units of $\mathfrak{R}$ to be 1/s.

Reaction	A	n [–]	T_a [K]
Atom-atom	1.8247×10^{-12}	3.597	69940
Atom-electron	7.407×10^{4}	1.511	141480

Table 2.1: Forward Arrhenius law parameters.

Reaction	A	n [–]	T_a [K]
Atom-atom	5.6655×10^{-11}	2.097	-112944
Atom-electron	2.2997×10^{6}	0.011	-41404

Table 2.2: Backward Arrhenius law parameters.

Furthermore, under a MT approach each forward and backward mechanism are supposed to evolve at a specific temperature. Two temperature bath are considered in the Argon 3 model, the electron temperature T_e (vibrational temperature) and a common heavy temperature T_h (translational temperature), Scoggins [45] provides a description of typical reaction temperatures for many reaction types. The reaction-dependent temperatures for the Argon 3 model used in this work are summarised in Table. 2.3.

Reaction	T_f	T_b
Atom-atom	T_h	T_h
Atom-electron	T_e	T_e

Table 2.3: Forward and backward reaction temperatures for the Argon 3 model.

Lastly, the Argon 3 model is composed of only monoatomic species, the heat capacity ratio γ is then considered to be the same for all species and is 5/3. This follows the recommendations from [31] in which $\gamma_e = 5/3$. Note that it is also considered that γ does not vary with temperature. Furthermore, the temperature state function derived in the previous chapter in Eq. (1.16) is slightly modified in the case of heavy species since they share a common temperature. The heavy temperature T_h is then computed from the sum of total energies of all heavy species, to distinguish from the overall set of pseudo-species, the $\mathcal{H}$ set is introduced referring then to the subset of heavy species in the mixture set $\mathcal{S}_3$.

$$\begin{aligned} \rho_h E_h = \sum_{\alpha \in \mathcal{H}} \rho_\alpha E_\alpha = \sum_{\alpha \in \mathcal{H}} \left(\frac{n_\alpha k_B T_h}{\gamma - 1} + \frac{1}{2} \rho_\alpha u_\alpha^2 \right) \\ \downarrow \\ T_h = \frac{(\gamma - 1)}{k_B} \frac{\sum_{\alpha \in \mathcal{H}} \rho_\alpha E_\alpha - \frac{1}{2} \rho_\alpha u_\alpha^2}{\sum_{\alpha \in \mathcal{H}} n_\alpha} \end{aligned} \tag{2.9}$$

2.2 Inelastic collision modeling

In the Argon 3 model previously described, only collisional chemical reactions are considered. These reactions are inelastic in nature as some energy is lost in the process. The production rates follow the Law of mass action, in the general case one can consider that the exchange in mass is a balance between how many particle are created and destroyed for a given reaction. When summing over each reaction in the set of reactions $\mathcal{R}$, this balance can be called the net

production rate, here expressed in $1/\mathrm{m}^3$. The net production rates are computed as defined in [45], note that no third body reactions are present in the Argon 3 model.

$$\dot{\omega}_\alpha^{(n)} = \frac{M_\alpha}{m_\alpha} \sum_{r \in \mathcal{R}} \left(\nu''_{\alpha,r} - \nu'_{\alpha,r}\right) \left[k_{f,r}\left(T_{f,r}\right) \prod_{\beta \in \mathcal{S}} \left(\frac{\rho_\beta}{M_\beta}\right)^{\nu'_{\beta,r}} - k_{b,r}\left(T_{b,r}\right) \prod_{\beta \in \mathcal{S}} \left(\frac{\rho_\beta}{M_\beta}\right)^{\nu''_{\beta,r}} \right] \tag{2.10}$$

To relate to the conserved variables of the conservation system defined in the previous chapter, one can express the molar concentration in function of particle density. The net production rates are then function of temperature and particle density.

$$\dot{\omega}_\alpha^{(n)} = \frac{M_\alpha}{m_\alpha} \sum_{r \in \mathcal{R}} \left(\nu''_{\alpha,r} - \nu'_{\alpha,r}\right) \left[k_{f,r}\left(T_{f,r}\right) \prod_{\beta \in \mathcal{S}} \hat{n}_\beta^{\nu'_{\beta,r}} - k_{b,r}\left(T_{b,r}\right) \prod_{\beta \in \mathcal{S}} \hat{n}_\beta^{\nu''_{\beta,r}} \right] \tag{2.11}$$

Here $\hat{n}_\beta = n_\beta / \mathrm{N}_a$ is the molar concentration of species β in function of its particle density, with N_a the Avogadro number. Moreover, the net production rate can be split into a contribution of the forward Γ_α^f and backward Γ_α^b production.

$$\dot{\omega}_\alpha^{(n)} = \underbrace{\frac{M_\alpha}{m_\alpha} \sum_{r \in \mathcal{R}} \left(\nu''_{\alpha,r} - \nu'_{\alpha,r}\right) k_{f,r}\left(T_{f,r}\right) \prod_{\beta} \hat{n}_\beta^{\nu'_{\beta,r}}}_{\equiv \Gamma_\alpha^f} - \underbrace{\frac{M_\alpha}{m_\alpha} \sum_{r \in \mathcal{R}} \left(\nu''_{\alpha,r} - \nu'_{\alpha,r}\right) k_{b,r}\left(T_{b,r}\right) \prod_{\beta} \hat{n}_\beta^{\nu''_{\beta,r}}}_{\equiv \Gamma_\alpha^b}$$

$$\Leftrightarrow$$

$$\dot{\omega}_\alpha^{(n)} = \Gamma_\alpha^f - \Gamma_\alpha^b$$

Let's remember that two reactions are considered in the Argon 3 model, in which the forward processes can be seen as ionization processes while backward processes as recombination processes. Therefore, the previously defined quantities Γ_α^f and Γ_α^b can be split further to express the contribution of each process for each reaction.

$$\Gamma_\alpha^f = \sum_{r \in \mathcal{R}} \Gamma_{\alpha,r}^f \Leftrightarrow \Gamma_\alpha^{ion} = \Gamma_{\alpha,(a-a)}^f + \Gamma_{\alpha,(a-e)}^f$$

$$\Gamma_\alpha^b = \sum_{r \in \mathcal{R}} \Gamma_{\alpha,r}^b \Leftrightarrow \Gamma_\alpha^{rec} = \Gamma_{\alpha,(a-a)}^b + \Gamma_{\alpha,(a-e)}^b$$

Here $(a-a)$ and $(a-e)$ refers respectively the atom-atom and atom-electron reactions defined in Eq. (2.2) and Eq. (2.1).

Having decomposed the production rates into forward and backward mass productions for each reactions, one can then define momentum and total energy exchanges related to chemical processes. To do so, it is first assumed that during an inelastic collision the created particles are emitted at the speed of the heaviest of the reactant species. This is quite a strong assumption and is based on a intuitive approach which can be illustrated as follows.
Let's take for example the forward reaction in the case of the atom-electron impact reaction Eq. (2.1). The chemical reaction occurs when an electron collides with a neutral with enough energy such as to trigger the reaction. The product of such reaction is that the excess of energy provides enough energy to extract an electron from the neutral atom. The neutrals becomes an ion and a free electron is emitted. It is then supposed that the velocity of these "created"[1] particles is the same as the neutral speed pre-collision. Furthermore, the free electron providing

[1]The term "create" is used here for a lack of better term as electron of ions are not in fact created but are the result of the extraction of an electron from a neutral atom.

the excess energy pre-collision is supposed to remain unperturbed in term of velocity. A similar reasoning can be done for the corresponding backward reaction. This time the difference is that a free electron and a ion recombine (or a free electron is absorbed by an ion). In this case, the "created" neutral atom inherits the speed of the ion, the reasoning behind it is that the major contribtuion to its momentum comes from the ion pre-collision since electron are much lighter. The above example can be summarized with the diagram in Fig. 2.1 detailling the states of each particle involved in the considered reaction before and after the collision.

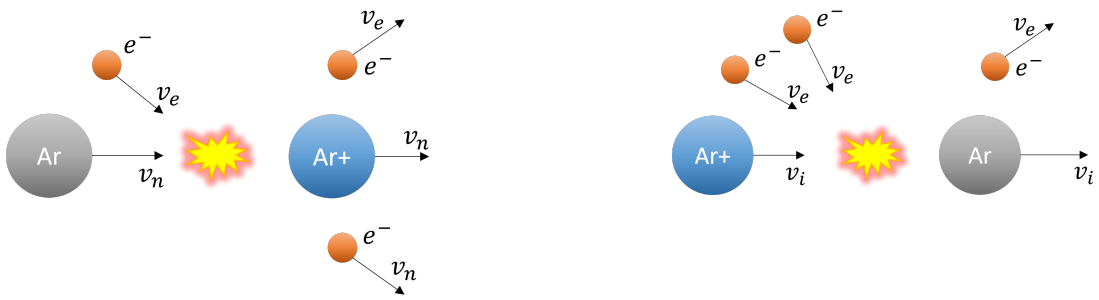

(a) Forward reaction.

(b) Backward reaction.

Figure 2.1: Diagram of the momentum of each species pre and post collision for the atom-electron impact reaction Eq. (2.1), the mass of each species is conserved while speed is indicated as v for each species.

Following this assumption, and generalizing to each reaction, one notices that the momentum production for ionization processess is driven by the neutral velocity while recombination processess by the ion velocity. Therefore, for each reaction the momentum production rate is defined as

$$\dot{\omega}_\alpha^{(m)} = \Gamma_\alpha^{ion} u_n - \Gamma_\alpha^{rec} u_i. \tag{2.12}$$

Similarly, the total energy production follows the same assumption done for the momentum production in regards to the kinetic energy production where the forward velocity is the neutral velocity and the backward velocity is the ion velocity. However, one alos needs to take into account the production of internal energy. The expression of it was developped in [35] for a binary mixture of ions and neutrals species. The expression can then be expanded to the current plasma model. For this work, the production of internal energy is then proportional to the reaction-dependent temperatures of Table. 2.3 for each reaction. Regrouping each contribution, the total energy production rate is then

$$\begin{aligned}\dot{\omega}_\alpha^{(e)} = &\frac{1}{2}\left(\Gamma_\alpha^{ion} u_n^2 - \Gamma_\alpha^{rec} u_i^2\right) \\ &+ \frac{1}{\gamma - 1}\frac{k_B}{m_\alpha}\left(\Gamma^f_{\alpha,(a-a)} T_h + \Gamma^f_{\alpha,(a-e)} T_e - \Gamma^b_{\alpha,(a-a)} T_h - \Gamma^b_{\alpha,(a-e)} T_e\right).\end{aligned} \tag{2.13}$$

2.3 Elastic collision modeling

Elastic collisions are modeled following a collision model between two bodies each with their own mass and speed. The post collision velocities are then described through conservation of momentum and kinetic energy. For notation purpose, the speed pre-collision will be denoted by u_k while after collision by v_k. Take then two particles denoted by the subscript α and β, the conservation equations are then

$$\begin{aligned} m_\alpha u_\alpha + m_\beta u_\beta &= m_\alpha v_\alpha + m_\beta v_\beta \\ m_\alpha u_\alpha^2 + m_\beta u_\beta^2 &= m_\alpha v_\alpha^2 + m_\beta v_\beta^2. \end{aligned} \tag{2.14}$$

The post-collision velocities v_α, v_β are obtained by solving the above system in function of u_α and u_β.

$$\begin{aligned} v_\alpha &= \frac{m_\alpha - m_\beta}{m_\alpha + m_\beta} u_\alpha + \frac{2m_\beta}{m_\alpha + m_\beta} u_\beta \\ v_\beta &= \frac{2m_\alpha}{m_\alpha + m_\beta} u_\alpha + \frac{m_\beta - m_\alpha}{m_\alpha + m_\beta} u_\beta \end{aligned} \tag{2.15}$$

The gain of momentum of a particle α collinding with another particle β is computed as

$$\Delta \left(mV\right)_\alpha = m_\alpha \left(v_\alpha - u_\alpha\right) = 2 \frac{m_\alpha m_\beta}{m_\alpha + m_\beta} \left(u_\beta - u_\alpha\right) = 2\, m_{\alpha\beta} \left(u_\beta - u_\alpha\right).$$

One can now extrapolate this expression to describe the exchange of momentum due to elastic collision of a particular species α when colliding with another species β. The total exchange of momentum per second is then proportional to the number of collision occurring in a second, in other words it is proportional the particle density of species α and the collision frequency $\nu_{\alpha\beta}$ between species α and β.

$$r_{\alpha\beta}^{(m)} = \Delta \left(mV\right)_\alpha n_\alpha \nu_{\alpha\beta} = 2\, m_{\alpha\beta} \left(u_\beta - u_\alpha\right) n_\alpha \nu_{\alpha\beta} \tag{2.16}$$

Summing all exchanges between all species β gives then the total production of momentum for particle α due to elastic collisions. Note that collision between the same species result in a zero exchange of momentum as expected.

Similar to momentum exchanges, the gain of kinetic energy can be computed from the post-collision velocities.

$$\begin{aligned} \frac{1}{2}\Delta \left(mV^2\right)_\alpha &= \frac{1}{2} m_\alpha \left(v_\alpha^2 - u_\alpha^2\right) \\ &= \frac{1}{2} m_\alpha \left(v_\alpha + u_\alpha\right) \left(v_\alpha - u_\alpha\right) \\ &= \frac{1}{2} \left(v_\alpha + u_\alpha\right) \Delta \left(mV\right)_\alpha \\ &= \left(\frac{m_{\alpha\beta}}{m_\alpha} u_\beta + \frac{m_{\alpha\beta}}{m_\beta} u_\alpha\right) \Delta \left(mV\right)_\alpha \end{aligned}$$

Likewise to the inelastic collision modeling, one must also include exchanges of internal energy through elastic collision to get the exchange of total energy. The exchange of internal energy is in practice proportional to the difference in temperature between the two colliding particles. The computation of it follows the work done in [5] and is thus

$$\Delta \left(m\mathcal{U}\right)_\alpha = 3\, \zeta_{\alpha\beta} m_{\alpha\beta} k_B \left(T_\beta - T_\alpha\right).$$

where $\zeta_{\alpha\beta}$ is defined as the ratio of energy to momentum transfer. This ratio will be defined in the next section as it depends on the ratio of energy to momentum transfer cross-sections.
Finally, adding both contributions and multiplying by the number of collision per second and the particle density of species α, the total production of energy due to elastic collisions is the following.

$$\begin{aligned} r_{\alpha\beta}^{(e)} &= \left[\Delta \left(m\mathcal{U}\right)_\alpha + \frac{1}{2}\Delta \left(mV^2\right)_\alpha\right] n_\alpha \nu_{\alpha\beta} \\ &= \left(\frac{m_{\alpha\beta}}{m_\alpha} u_\beta + \frac{m_{\alpha\beta}}{m_\beta} u_\alpha\right) r_{\alpha\beta}^{(m)} + 3\, \zeta_{\alpha\beta} m_{\alpha\beta} k_B \left(T_\beta - T_\alpha\right) n_\alpha \nu_{\alpha\beta} \end{aligned} \tag{2.17}$$

Again, summing over all exchanges between all species β in the mixture gives then the total production of total energy for particle α.

2.4 Chemical properties

In this last section, the definition of the collision frequency and heat conductivity is done. As highlighted from the previous section, these parameters are key when describing the behaviour of the system of conservation equations Eqs. (1.11–1.12) and are dependent on the chemistry of the plasma mixture. In this work, the expression of such parameters is taken from litterature [5, 35, 42, 45, 49], in particular from the works of [5] which has detailled elastic collision for a plasma under a MF formulation and [35] for a low temperature collisionless plasma.

The collision frequency for elastic collision between species α and β is then,

$$\nu_{\alpha\beta} = n_\beta \, \sigma_{\alpha\beta} \sqrt{\frac{8}{\pi} \frac{k_B T_{\alpha\beta}}{m_{\alpha\beta}}} \tag{2.18}$$

where $\sigma_{\alpha\beta}$ and $T_{\alpha\beta}$ are respectively the momentum transfer cross-section and the average temperature of the two colliding particle. The average temperature is defined similarly as the reduced mass $m_{\alpha\beta}$ between particle α and β.

$$T_{\alpha\beta} = \frac{m_\beta T_\alpha + m_\alpha T_\beta}{m_\alpha + m_\beta} \tag{2.19}$$

This definition is taken from [35] and agrees with the expression derived from [5]. Similarly, the heat conductivity is taken from [35] ,

$$\kappa_\alpha = 4 \frac{n_\alpha k_B^2 T_\alpha}{m_\alpha \nu_\alpha} \tag{2.20}$$

where ν_α is the intra-species collision frequency. In this work this frequency is modeled with Eq. (2.18) for same species collision and is thus $\nu_\alpha = \nu_{\alpha\alpha}$. The heat flux is considered for all species but one can notice that because of the small mass of electron with respect to heavy species, the heat conductivity of electron is expected to be more important than heavy species.

An important parameter that still needs to be defined, as introduced in both definition of the collision frequency and heat flux is the momentum transfer cross-section $\sigma_{\alpha\beta}$. The computation of it is well described in literature [42, 49], in this work the computation follows the methodology presented in [5]. In practice, the momentum transfer cross-section is obtained by computing collision integrals between species α and β across scattering angles. However, it is often convenient to express collision integrals in terms of reduced collision integrals $\bar{Q}^{(l,s)}_{\alpha\beta}$. Where the parameter (l, s) correspond to the Sonine polynomial coefficients used in the Chapman-Enskog solution procedure [42]. Moreover, these reduced collision integrals can understood as the deviation from the rigid-sphere values and are often used since they have a weaker dependence on temperature.
Therefore, the choice was made to consider the momentum transfer cross-section to be estimated by $\bar{Q}^{(1,1)}_{\alpha\beta}$, which is often used in kinetic theory of gases [40]. The computation of $\bar{Q}^{(1,1)}_{\alpha\beta}$ can be done with the MUTATION^{++} library and is shown in Fig. 2.2 for all possible collisions in the Argon 3 model and for different temperature regimes.

Before ending this chapter, let's remember that one last term was introduced during the elastic collision modeling, the energy to momentum transfer coefficient $\zeta_{\alpha\beta}$ Eq. (2.17). Benilov [5] defines it from the ratio of energy transfer cross-section $Q^{(e)}_{\alpha\beta}$ to momentum transfer cross-section $Q^{(m)}_{\alpha\beta}$. Various definitions are possible, for this work the definition follows the

expression for rigid spheres particles.

$$\zeta_{\alpha\beta} \equiv \frac{Q^{(e)}_{\alpha\beta}}{Q^{(m)}_{\alpha\beta}} = 1 + \frac{2}{3} M^2_{\alpha\beta} \tag{2.21}$$

Here $M_{\alpha\beta}$ is the Mach number of the relative motion between species α and β defined as

$$M_{\alpha\beta} = \sqrt{\frac{m_{\alpha\beta}}{2kT_{\alpha\beta}}}\, |u_\alpha - u_\beta| \,. \tag{2.22}$$

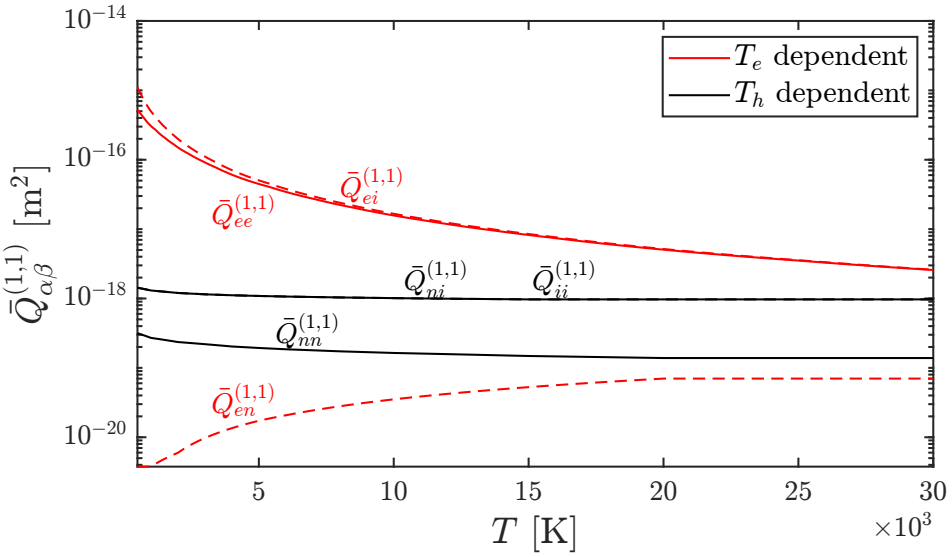

Figure 2.2: Average collision cross-section from MUTATION^{++} , dashed lines correspond to inter-species collisions and full lines to intra-species collisions, subscripts n, i and e refer respectively to neutrals, ions and electrons species.

Chapter 3

Application to a 1D post shock relaxation problem

In this chapter an application is selected for the governing equations derived in the first chapter of this work. The considered test case is a one dimensional post shock relaxation problem of an argon plasma, for ease of reference the test case will be referred as the 1D post-shock relaxation problem from now on. Furthermore, the argon plasma mixture is modeled with the Argon 3 model developed in the second chapter of this work.

For reference, this problem is based on the work of UTIAS [46] and Kapper [31]. The first paper provides experimental data as well as numerical resolutions with a simple mixture model (similar to the Argon 3 model) under a Multi-component (MC) formulation of the problem. On the other hand, [31] has solved the equations (MC) with a more complex mixture taking into account different levels of excitation for heavy species, such model is called a State-to-State model (STS). In comparison to the Argon 3 model, the STS model in [31] is composed of 34 species. For this work, the results of [46] will be used as the primary reference for solution of this work while the results of [31] will be used to assess the Argon 3 model performance. Furthermore, this problem has also been tackled by [4, 7].

In the first part of this chapter, the problem is presented according to [46] and important aspects of the problem are unveiled. Then, the equations are scaled with relevant scales to obtain an non-dimensional formulation of the governing equations Eqs. (1.10–1.12). Finally, a mathematical study of the adimensional system of equations to be solved numerically is done and appropriate boundary and initial conditions are chosen. At the end of this chapter, the goal will be to gain insight on the challenges of the problem.

3.1 The 1D post-shock relaxation problem definition

The 1D post-shock relaxation problem is an argon plasma relaxation problem. The test case at hand consist in the study of an argon gas in a shock tube. Experimentally, an argon gas is maintained at different densities left and right of a diaphragm in a tube. The diaphragm is then broken at $t = 0\,\mathrm{s}$ and a shock occurs at the location of the broken diaphragm. The experimental data and reference solution is taken from [46], in particular, this work focuses of the test case labeled No. 2.

For this test case, the gas in the region left of the shock is not ionized, the Mach number is 15.9, moreover the gas pressure and temperature in the left region are respectively 685.3 Pa and 293.6 K. The temperature after the shock jumps to 23452 K, under such conditions ionization

processes start occurring and the gas turns into a plasma. The ionization of the gas occurs within a certain length after the shock and eventually the plasma reaches a thermal equilibrium at a position $x_E \sim 2\,\text{cm}$ from the shock, the plasma relaxes then up to the conditions right of the shock before the diaphragm was broken.

The problem consists then in solving for the ionization structure and determining the location of x_E. The problem becomes steady in the one dimensional case if considering the shock to be stationary. To do so, the reference frame of the solution is set to be the moving shock reference frame, the shock is then located at $x = 0\,\text{m}$ and x measures the distance from the shock. The reference steady solution is shown in Fig. 3.1. Additionally, one can split the domain into several zones and relate them to different processes occurring during the ionization of the argon gas. These zones are shown in Fig. 3.1a, five zone can then be identified:

- Zone I, where the absence of free electrons and the high heavy temperature starts the ionization of the gas through atom-atom impact ionization reactions.
- Zone II, where enough free electrons are present to trigger atom-electron impact ionization reactions.
- Zone III, the temperature of electrons slowly rises from exchange of internal energy with heavies through elastic collision balanced by inelastic processes.
- Zone IV, the electron avalanche zone, where the build up in free electron reaches a level such as recombination processes dominate, in particular the atom-electron recombination reaction (three-body recombination).
- Zone V, the relaxation zone, where the plasma has reached thermal equilibrium and no production of particle occurs. The mixture then relaxes up to conditions far away downstream of the shock tube.

The quantity of interest for this problem are the total plasma mass density and the particle densities of each species, the mixture velocity and the temperature profiles. Total quantities are defined as follows. The mixture particle density is the sum of particle densities of each species in the mixture.

$$n = \sum_{\beta \in \mathcal{S}} n_\beta \tag{3.1}$$

Similarly, the total mass density is the sum of the mass densities which are defined from the particle densities of each species.

$$\rho = \sum_{\beta \in \mathcal{S}} m_\beta n_\beta \tag{3.2}$$

Lastly, the speed of mixture is defined from the previous relations.

$$u = \frac{1}{\rho} \sum_{\beta \in \mathcal{S}} \rho_\beta u_\beta \tag{3.3}$$

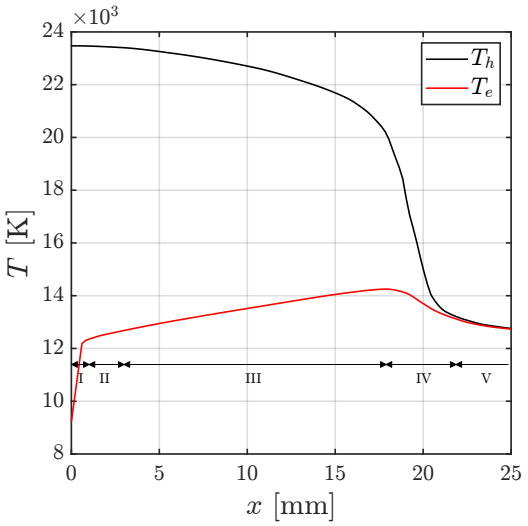

(a) Post-shock structure close to the shock with zones I to V as detailed in [31].

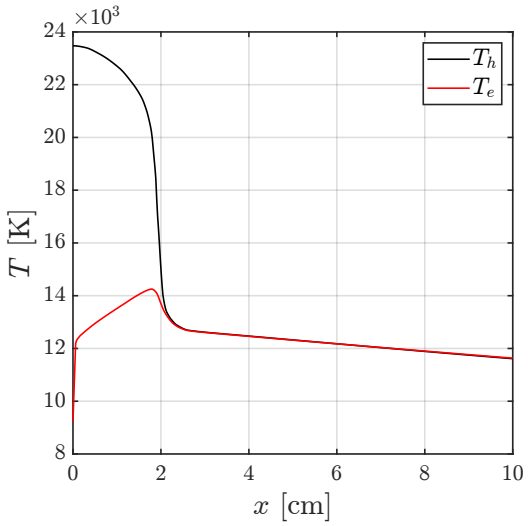

(b) Temperature profiles over the domain.

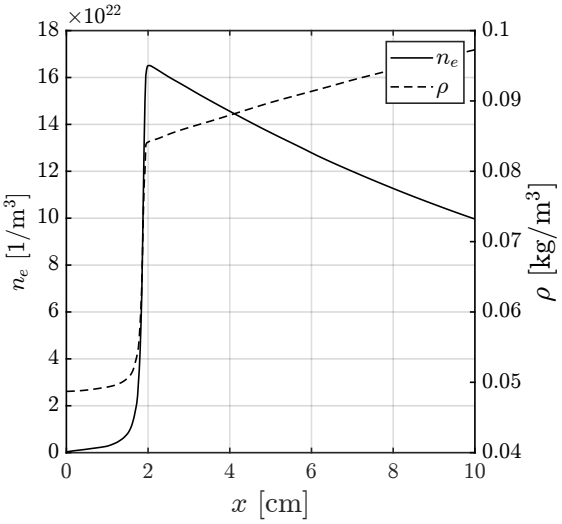

(c) Total plasma density ρ and electron particle density n_e over the domain.

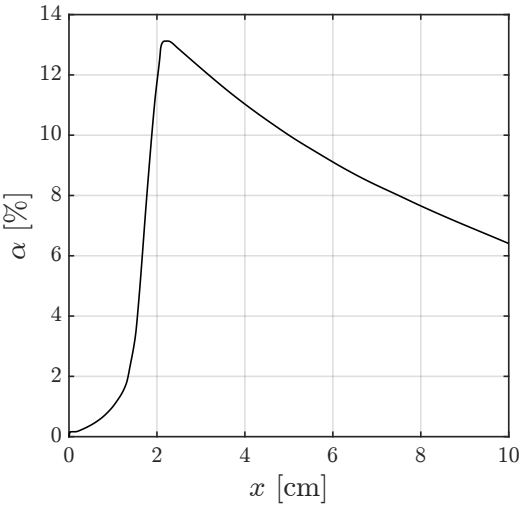

(d) Ionization fraction $\alpha = n_e/n$ over the domain.

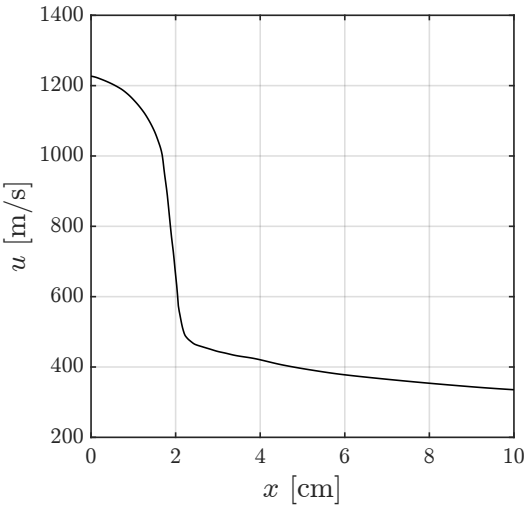

(e) Plasma mixture speed over the domain.

Figure 3.1: Reference solution [46] for the 1D post-shock relaxation problem.

Furthermore, Table. 3.1 summarize important parameters of the problem, in particular the pre-shock conditions of the argon gas. To determine the post-shock conditions (initial conditions) of the problem, the strategy is to freeze the chemistry through the shock and compute the post-shock conditions using the Rankine-Hugoniot jump relations for steady and normal shocks. These relations are recapitualed in Appendix. A. Moreover, it is assumed that only the translational temperature T_h jumps after the shock, the vibrational temperature T_e is therefore assumed to remain at its pre-shock value. Lastly, the chemistry pre-shock is determined by computing the molar concentration X_i of each species from equilibrium relations. To do so, one can use the MUTATION^{++} tool `mppequil`. The post-shock conditions are then summarized in Table. 3.2.

Parameter	**Unit**	**Value**
Length of domain, L	m	0.1
Electron-to-Heavy mass ratio, ε	–	1.373×10^{-5}
Relaxation temperature, T_r	K	11632
Pre-shock mach, M_∞	–	15.9
Pre-shock pressure, p_∞	Pa	685.28
Pre-shock temperature, T_∞	K	293.6
Pre-shock electron molar concentration, X_{e^-}	–	0
Pre-shock neutral molar concentration, X_{Ar}	–	1
Pre-shock ion molar concentration, X_{Ar^+}	–	0

Table 3.1: Post shock relaxation test case important parameters.

M_1 [–]	p_1 [kPa]	T_1 [K]	$T_{1,h}$ [K]	$T_{1,e}$ [K]	n_1 [1/m^3]	V_1 [m/s]
0.45	216.385	23452	23452	293.6	7.34×10^{23}	1226.8

Table 3.2: Post shock conditions after shock located at $x = 0$ m obtained with the Rankine-Hugoniot steady normal shock relations and frozen chemistry.

3.2 Scaling and adimensional equations

In this section, the scaling of Eqs. (1.10–1.12) is done. One must take particular interest in the choice of scales as difference in orders of magnitudes between conserved variables will influence the accuracy of the computation. In this case, one must consider the difference in orders of magnitude between the momentum and total energy as well as between heavy species and electrons.

Some reference scales are first chosen based on the considered problem, a scale for length $L_0 = 1\,\text{m}$, mass $m_0 = m_h$, number density $n_0 = n_1$ and temperature $T_0 = T_r$. The other scales can be derived from these reference scales. The velocity scale of a given species α is computed as the thermal speed; this choice is made as the square of the thermal speed is a good estimate of the internal energy (which in this problem is the main contributor to the total energy) and is consistent with the scaling of the kinetic contribution (which is directly the square of the velocity scale).

$$u_{0,\alpha} = \sqrt{\frac{k_B\, T_0}{m_\alpha}} \tag{3.4}$$

However, taking $u_{0,\alpha}$ as a velocity scale might be not optimal as the orders of the thermal speeds of each species vary greatly and the velocities in the post-shock problem do not.

$$\mathcal{O}\left(u_{0,e}\right) = 10^6 \;\gg\; \mathcal{O}\left(u_{0,h}\right) = 10^3 \sim \mathcal{O}\left(u_{\alpha}\right)$$

Therefore, a unique velocity scale is preferred. In this case, the thermal speed of the neutrals is taken as it is much more close to the actual speed of the mixture in the problem. Having defined a unique velocity scale, one can define a characteristic time scale and frequency scale with the length scale.

$$u_0 = \sqrt{\frac{k_B\, T_0}{m_0}} = 1555.9 \text{ m/s}$$

$$t_0 = \frac{L_0}{u_0} = 64.272 \times 10^{-5} \text{ s}$$

$$\nu_0 = \frac{1}{t_0} = 1555.9 \text{ Hz}$$

Moreover, since the total energy is the sum of internal and kinetic energy, and as mentioned before a good estimation of the internal energy is the squared thermal speed, the total energy scale can be chosen to be $u_{0,\alpha}^2$. From here, all other relevant scales can be computed from the previously defined ones.

$$E_{0,\alpha} = u_{0,\alpha}^2$$

$$p_0 = n_0 k_B T_0 = 117.92 \text{ kPa}$$

$$H_{0,\alpha} = E_{0,\alpha} + \frac{p_0}{n_0 m_\alpha} = E_{0,\alpha} + u_{0,\alpha}^2 \sim u_{0,\alpha}^2$$

Rearranging the system of governing equation, the adimensional form of Eqs. (1.10–1.12) can be obtained by developing each term and expressing it in adimensional form. For this purpose, adimensional quantities will be denoted with the $\tilde{a}$ notation where a is a given physical quantity. The scales associated to each equations are then

$$\frac{n_0}{t_0}, \quad \frac{n_0 u_0}{t_0} \quad \text{and} \quad \frac{n_0 u_{0,\alpha}^2}{t_0} = \frac{n_0 E_{0,\alpha}}{t_0}$$

respectively for the particle density, momentum and total energy equation. To get an adimensional system, the scaling of each term in a given equation will need to be consistent to the corresponding equation scale. Let's then develop the spatial and source terms for each equation by highlighting their respective scales. The pressure and the total energy convective flux are the following.

$$\partial_x \left(\frac{p_\alpha}{m_\alpha}\right) = \frac{p_0}{L_0}\frac{1}{m_\alpha}\partial_{\tilde{x}}\tilde{p}_\alpha = \frac{n_0 k_B T_0}{u_0 t_0}\frac{1}{m_\alpha}\partial_{\tilde{x}}\tilde{p}_\alpha = \frac{n_0 u_0}{t_0}\frac{m_0}{m_\alpha}\partial_{\tilde{x}}\tilde{p}_\alpha = \frac{n_0 u_0}{t_0}\partial_{\tilde{x}}\left(\frac{\tilde{p}_\alpha}{\tilde{m}_\alpha}\right) \tag{3.5}$$

$$\partial_x \left(n_\alpha H_\alpha u_\alpha\right) = \frac{n_0 E_{0,\alpha} u_0}{L_0}\partial_{\tilde{x}}\left(\tilde{n}_\alpha \tilde{H}_\alpha \tilde{u}_\alpha\right) = \frac{n_0 E_{0,\alpha}}{t_0}\partial_{\tilde{x}}\left(\tilde{n}_\alpha \tilde{H}_\alpha \tilde{u}_\alpha\right) \tag{3.6}$$

Regarding the heatflux, a scale for the heat conductivity can be defined following the expression derived in the previous chapter in Eq. (2.20). The scale is then

$$\kappa_{0,\alpha} = \frac{5}{2}\frac{n_0 k_B^2 T_0}{m_\alpha \nu_0} \tag{3.7}$$

and the adimensional heatflux can be shown to be consistent with the energy equation scale.

$$\begin{aligned}\frac{1}{m_\alpha}\partial_x\left(\kappa_\alpha\partial_x T_\alpha\right) &= \frac{1}{m_\alpha}\frac{\kappa_{0,\alpha}T_0}{L_0^2}\partial_{\tilde{x}}\left(\tilde{\kappa}_\alpha\partial_{\tilde{x}}\tilde{T}_\alpha\right)\\ &= \frac{n_0}{t_0}\left(\frac{u_{0,\alpha}^2}{u_0}\right)^2\partial_{\tilde{x}}\left(\tilde{\kappa}_\alpha\partial_{\tilde{x}}\tilde{T}_\alpha\right)\\ &= \frac{n_0 u_{0,\alpha}^2}{t_0}\left(\frac{m_0}{m_\alpha}\right)\partial_{\tilde{x}}\left(\tilde{\kappa}_\alpha\partial_{\tilde{x}}\tilde{T}_\alpha\right)\\ &= \frac{n_0 E_{0,\alpha}}{t_0}\partial_{\tilde{x}}\left(\frac{\tilde{\kappa}_\alpha}{\tilde{m}_\alpha}\partial_{\tilde{x}}\tilde{T}_\alpha\right)\end{aligned} \tag{3.8}$$

Finally, considering the source term scales to be the same as the equation scales by definition ensure a consistent scaling for the source terms.

Injecting back all the previous expressions and dividing each equation by its scale, the adimensional system of equations is obtained.

$$\begin{aligned}\partial_{\tilde{t}}\tilde{n}_\alpha + \partial_{\tilde{x}}\left(\tilde{n}_\alpha\tilde{u}_\alpha\right) &= \tilde{S}_\alpha^{(n)}\\ \partial_{\tilde{t}}\left(\tilde{n}_\alpha\tilde{u}_\alpha\right) + \partial_{\tilde{x}}\left(\tilde{n}_\alpha\tilde{u}_\alpha^2 + \frac{\tilde{p}_\alpha}{\tilde{m}_\alpha}\right) &= \tilde{S}_\alpha^{(m)}\\ \partial_{\tilde{t}}\left(\tilde{n}_\alpha\tilde{E}_\alpha\right) + \partial_{\tilde{x}}\left(\tilde{n}_\alpha\tilde{H}_\alpha\tilde{u}_\alpha\right) &= -\partial_{\tilde{x}}\left(\frac{\tilde{\kappa}_\alpha}{\tilde{m}_\alpha}\partial_{\tilde{x}}\tilde{T}_\alpha\right) + \tilde{S}_\alpha^{(e)}\end{aligned} \tag{3.9}$$

Note that for $\alpha = e$, $\tilde{m}_\alpha = \varepsilon$ and for $\alpha \in \mathcal{H}$, $\tilde{m}_\alpha = 1$ since the neutral and ion mass are almost the same in this problem ($m_n \approx m_i$). Additionally to avoid clutter, the $\tilde{a}$ notation referring to non-dimensional quantities will be dropped for the rest of this work. Any quantity should then be assumed to be non-dimensional by default except if specified otherwise.

3.3 Characteristic analysis

Having descibed the problem in an adimensional form, it is then useful to perform a characteric analysis to better understand the underlying challenges of the problem form a mathematical point of vue. Let's first write the adimensional system in matrix form,

$$\partial_t\boldsymbol{U} + \partial_x\boldsymbol{F}^c + \partial_x\boldsymbol{F}^d = \boldsymbol{S} \tag{3.10}$$

where $\boldsymbol{U}$, $\boldsymbol{F}^c$, $\boldsymbol{F}^d$ and $\boldsymbol{S}$ are respectively the vectors grouping all species for the conserved variables, the convective fluxes, the diffusive fluxes and the source terms. The characterics of the system are driven by the convective part of the system, one can show that the slopes of the caracteristics of the system are the eigenvalues of the convective flux jacobian matrix $\boldsymbol{A}^c$ with respect to the conserved variables.

$$\boldsymbol{A}^c = \frac{\partial\boldsymbol{F}^c}{\partial\boldsymbol{U}} \tag{3.11}$$

Before computing $\boldsymbol{A}^c$, let's first notice that ordering the conserved variables in a certain way can easily simplify the process. Indeed choosing the following ordering for the conserved variable vector,

$$\boldsymbol{U} = \begin{bmatrix}\boldsymbol{U}_e\\ \boldsymbol{U}_n\\ \boldsymbol{U}_i\end{bmatrix}$$

implies $\boldsymbol{A}^c$ to be in the following form.

$$\boldsymbol{A}^c = \begin{bmatrix} \boldsymbol{A}_e^c & \mathbf{0} & \mathbf{0} \\ \mathbf{0} & \boldsymbol{A}_n^c & \mathbf{0} \\ \mathbf{0} & \mathbf{0} & \boldsymbol{A}_i^c \end{bmatrix}$$

Since the subsystem of each species in the mixture are only coupled through the source terms. One can then show that the eigenvalues of the complete system are the combined eigenvalues of each subsystem associated to each species.

$$\det\left(\boldsymbol{A}^c - \lambda \mathbf{I}_9\right) = 0 \;\Leftrightarrow\; \prod_{\alpha \in \mathcal{S}} \det\left(\boldsymbol{A}_\alpha^c - \lambda_\alpha \mathbf{I}_3\right) = 0 \tag{3.12}$$

Therefore, a general analysis of the matrix $\boldsymbol{A}_\alpha^c$ associated to the subsystem of species α can be done and will be valid for each species of the plasma mixture. In this case, the convective part of the system of species α is the same as the 1D Euler equations with the only difference being that the first conserved variable is the particle density instead of mass density. Therefore, the characteristics analysis follows the 1D Euler characteristic analysis. In this section only the important aspects of it will be explored but a more complete analysis is done in Appendix. B. The fluxes and jacobian matrix associated to each species system is the following.

$$\boldsymbol{U}_\alpha = \begin{bmatrix} n_\alpha \\ n_\alpha u_\alpha \\ n_\alpha E_\alpha \end{bmatrix} \qquad \boldsymbol{F}_\alpha^c = \begin{bmatrix} n_\alpha u_\alpha \\ n_\alpha u_\alpha + \frac{p_\alpha}{m_\alpha} \\ n_\alpha H_\alpha u_\alpha \end{bmatrix}$$

$$\boldsymbol{A}_\alpha^c = \frac{\partial \boldsymbol{F}_\alpha^c}{\partial \boldsymbol{U}_\alpha} = \begin{bmatrix} 0 & 1 & 0 \\ -\frac{(\gamma-3)}{2} u_\alpha^2 & (3-\gamma)\, u_\alpha & \frac{(\gamma-1)}{m_\alpha} \\ -\gamma E_\alpha u_\alpha + (\gamma-1)\, u_\alpha^3 m_\alpha & \gamma E_\alpha - \frac{(\gamma-3)}{2} u_\alpha^2 m_\alpha & \gamma u_\alpha \end{bmatrix}$$

Solving equation Eq. (3.12) for $\boldsymbol{A}_\alpha^c$, the eigenvalues associated to the species α are found.

$$\begin{aligned} \lambda_{\alpha,0} &= u_\alpha - c_\alpha \\ \lambda_{\alpha,1} &= u_\alpha \\ \lambda_{\alpha,2} &= u_\alpha + c_\alpha \end{aligned}$$

Furthermore, from the diagonlization property of inversible matrices $\boldsymbol{A}_\alpha^c = \boldsymbol{R}_\alpha^{-1} \boldsymbol{\Lambda}_\alpha \boldsymbol{R}_\alpha$, the right eigenvectors matrix $R_{\alpha,i}$ are found. Here $\boldsymbol{\Lambda}_\alpha$ is the diagonal matrix formed by the eigenvalues of the system.

$$\boldsymbol{R}_\alpha = \begin{bmatrix} \boldsymbol{R}_{\alpha,0} & \boldsymbol{R}_{\alpha,1} & \boldsymbol{R}_{\alpha,2} \end{bmatrix} = \begin{bmatrix} 1 & 1 & 1 \\ u_\alpha - c_\alpha & u_\alpha & u_\alpha + c_\alpha \\ H_\alpha - u_\alpha c_\alpha m_\alpha & \frac{1}{2} u_\alpha^2 m_\alpha & H_\alpha + u_\alpha c_\alpha m_\alpha \end{bmatrix}$$

Finally, the caracteristics of the system of species α are

$$\begin{aligned} \frac{dp_\alpha}{m_\alpha} - n_\alpha c_\alpha\, du_\alpha = 0 \;\text{ for }\; \frac{dx}{dt} &= u_\alpha - c_\alpha \\ \frac{dp_\alpha}{m_\alpha} - c_\alpha^2\, dn_\alpha = 0 \;\text{ for }\; \frac{dx}{dt} &= u_\alpha \\ \frac{dp_\alpha}{m_\alpha} + n_\alpha c_\alpha\, du_\alpha = 0 \;\text{ for }\; \frac{dx}{dt} &= u_\alpha + c_\alpha. \end{aligned} \tag{3.13}$$

In the context of the 1D post relaxation problem defined previously, the temperature evolves between ~ 300 K and ~ 23400 K. Since the speed of sound c_α is closely linked to temperature as

shown in Eq. (1.18), one can bound the eigenvalues to a certain range depending on the regime of temperature of the problem. Doing so, it is observed that the first eigenvalue is always negative as $|u_\alpha| \leq c_\alpha$. Therefore, the first characteristic of the system will always propagate information from the outlet to the inlet of the domain.
Moreover, the magnitude of the eigenvalues for each species will differ, in particular for the electrons as the speed of sound of the electron is much greater than for heavy species. The problem is therefore very stiff and should be properly addressed in the numerical scheme.
Lastly, the strong difference in speeds of sound coupled with the fact that the velocities of each species should not vary much, implies then that the Mach number of each species will also differ greatly. Indeed, it is observed that the Mach number for heavy species is M_1 while for electron the Mach number is quite low ~ 0.003. This last feature will also need to be properly addressed in the numerical scheme as capturing phenomena for such low Mach can become problematic.

3.4 Boundary conditions

Boundary conditions are fundamental to properly solve flow equations. Without them, the solution is almost guaranteed to be wrong regardless on how accurate the numerical schemes is. Therefore, it is important to characterise the boundary conditions of the problem at hand. In practice one can express which physical quantities have to be imposed at the boundary of the domain by means of a characteristic analysis of the system. Indeed, the study of the characteristics allows to better understand how information is propagated through the domain. In general characteristics entering the domain propagate a certain physical quantity (through its conservation) from the exterior of the domain. Therefore, boundary conditions need to communicate to the solution inside the domain the quantities conserved on the entering characteristics.

Let's then take the characteristics obtained in the previous section in equation Eq. (3.13). As mentioned previously in Sec. 3.3, the first characteristic associated to the eigenvalue $u_\alpha - c_\alpha$ of the system for each species propagate from the outlet to the inlet (reverse from the flow). One can then conclude that two characteristics are entering the domain at the inlet while a single one is entering the domain at the outlet; fixing then the number of physical quantities to be imposed on each boundary. It is then common practice to choose such quantities based on a primitive decomposition of the system of conserved variables. For this problem the primitive variable are the following:

$$\boldsymbol{V} = \begin{bmatrix} n & u & p \end{bmatrix}^\intercal$$

Several combination of these variables are possible, since the system's characteristics are very similar to the classical Euler 1D characteristics the analysis of which combinations are valid will follow the Euler 1D case. Here the developments are not made but can be found in Appendix. B. The possible combinations are then summarised in Table. 3.3. Furthermore, the exact values to impose are taken from the reference steady-state solution shown in Fig. 3.1. The inlet values are computed from the post-shock conditions. The outlet values are taken at a reference length of 10 cm, in practice the domain's length could be expanded as in this problem the outlet boundary is not physical in the sense that the domain is cut arbitrarily along the tube's length (but far enough so that the ionization structure is clearly defined). The outlet values for this work are can then be found in Table. 3.4.

Boundary	Valid combinations	
Inlet	(n, p)	(n, u)
Outlet	(p)	(u)

Table 3.3: Boundary conditions possible combinations for the 1D post-shock relaxation problem.

n [1/m^3]	α [–]	u [m/s]	T [K]
1.5661×10^{24}	0.0636	335.384	11632

Table 3.4: Outlet solution state taken from reference solution at a location of $x = 10\,\text{cm}$ in Fig. 3.1, temperature and speed of each species are equal to the mixture value given here.

3.5 Initial conditions

Additionally, to boundary conditions one should also provide initial conditions. However, initial conditions differ from boundary conditions as the selection is mainly motivated by speed of resolution. Indeed for a steady problem like the 1D post shock relaxation problem, an initial conditions closer to the steady solution will favour the convergence rate and therefore the overall computation time.

On the other hand, even if a steady problem should not depend on time, some problem can depend on the evolution of the system. In short, such system need to go through an overshoot to be able to converge properly to the steady-state. For the problem at hand, the exact evolution in time is not known since the introduced modeling for the source terms has not been used in other studies. Therefore, the choosing of initial conditions is referred from literature and initial conditions for alike problems. Two possibility will be explored in this work.

The first is to consider uniform conditions with the post-shock values of Table. 3.2. Each species particle density is then calculated from their molar concentrations with respect to the mixture post-shock particle density n_1. The velocities are supposed all to be the mixture velocity V_1. The second alternative is to consider a profile varying between the post-shock state to the equilibrium state-state along the domain. The evolution from a state to another is done with a shifted sigmoid function acting as a logistic function and shifting from one state to another at a distance $x_s = 0.2\text{cm}$. The initial conditions for a given variable of the solution (n, u, T) is then,

$$u' = u'_{ps} + \frac{u'_{ss} - u'_{ps}}{1 + e^{-\frac{B}{L}(x - x_s)}} \tag{3.14}$$

where u' is the value of a given variable along the domain, u'_{ps} and u'_{ss} its values at respectively the post-shock state and the steady-state, and B is a scalar value allowing to module the strength of the sigmoid, for this problem it is set to a value of $60\,L$. A visualization of such initial conditions is shown in Fig. 3.2 and compared to the reference steady-state solution.

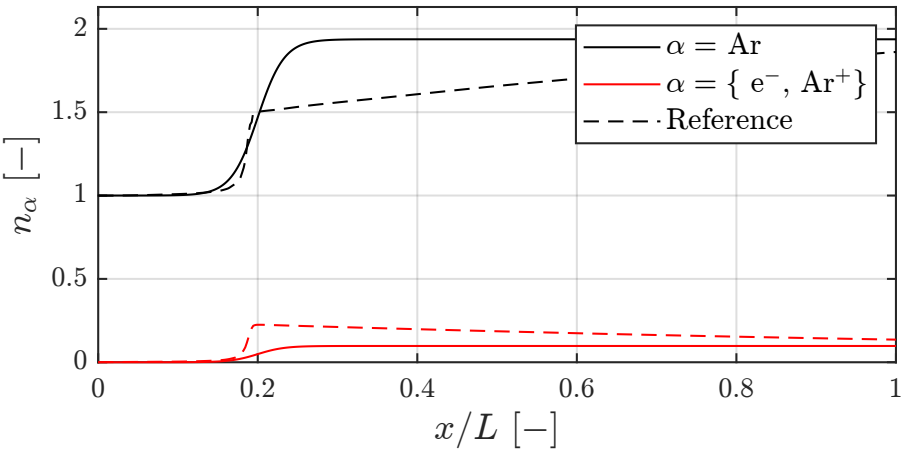

(a) Particle density profiles.

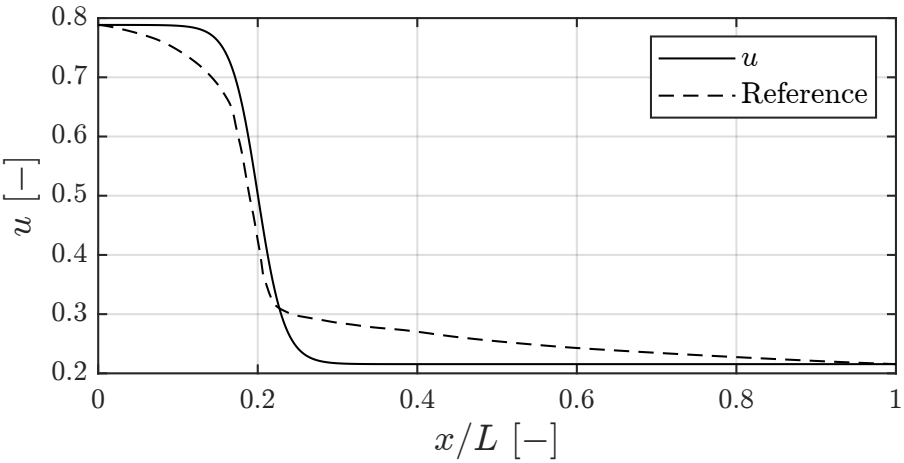

(b) Mixture velocity profile, each species is assumed to share the same profile.

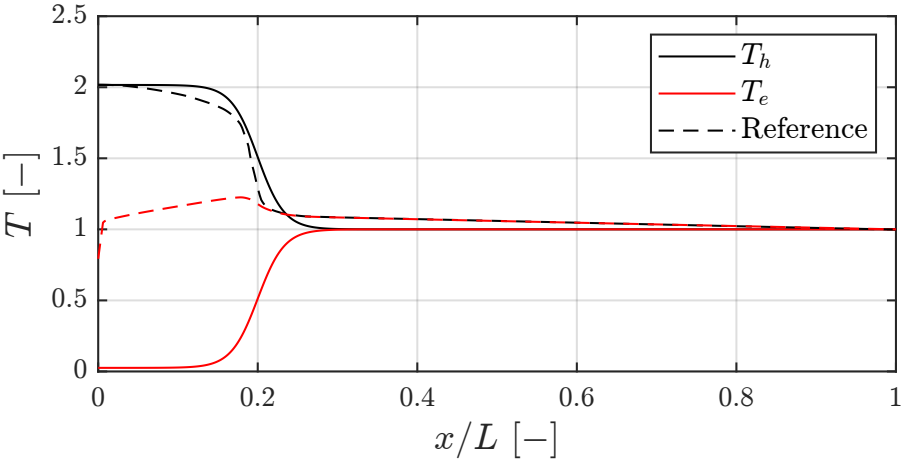

(c) Temperature profiles.

Figure 3.2: Second type of initial conditions with Eq. (3.14) compared to reference solution [46], non-dimensional quantities are given here according to the scaling done in Sec. 3.2.

Part II

Numerical methods

Chapter 4

The Discontinuous Galerkin Finite Element method

In this chapter, the Discontinuous Galerkin Finite Element Method (DG-FEM, DGM or even DG method for short) is presented and applied to the equation of the 1D post-shock relaxation problem. As the name suggest, the DG method is a finite element method using a discontinuous interpolation order with a Galerkin variational formulation. On key feature of DG method is that the solution is fully regular inside an element but not necessarly continuous across element, this property is also refered as the *broken trial space*. Such property allows a more flexible and easy construction of the shape function inside an element. Indeed, since no continuity is imposed, any basis funciton can be chosen to construct the shape functions. Additionally, this allows the interpolation order to be specific to the element allowing meshes with different interpolation orders per element.

In the first part of this chapter the method is presented for a general system of hyperbolic and elliptic equations. The general approach is then applied to the system of equation developed in the first chapter of this work.

4.1 Galerkin variational formulation

Let's first describe the Galerkin variation formulation for a general system of conservation laws. In the general one dimensional case, the system of equation has the following form:

$$\partial_t \boldsymbol{u}(x,t) + \partial_x \boldsymbol{F}\left(\boldsymbol{u}, \partial_x \boldsymbol{u}, x, t, \right) = \boldsymbol{S}(\boldsymbol{u}, x, t) \quad x \in \Omega, t \in \mathbb{R}^+ \tag{4.1}$$

where $\boldsymbol{u}$ is the unknowns (or the solution to be found), $\boldsymbol{F}$ the fluxes associated to the system which can be split into a contribution of convective $\boldsymbol{F}^c$ and diffusive fluxes $\boldsymbol{F}^d$, $\boldsymbol{S}$ the sources and lastly Ω the uni-dimensional domain.

A weak form formulation of Eq. (4.1) is found by multiplying it by a function $\varphi(x) \in C_1(\Omega)$ and integrating then over the domain Ω. Note for the following developments the dependence on x, t, etc of each term in Eq. (4.1) are not specified to avoid unnecessary clutter. The weak form of Eq. (4.1) is then

$$\int_\Omega \left(\partial_t \boldsymbol{u} - \boldsymbol{S}\right) \varphi \, dV - \int_\Omega \boldsymbol{F} \partial_x \varphi \, dV + \oint_{\partial\Omega} \boldsymbol{F} \cdot \boldsymbol{n} \varphi \, dS = 0 \tag{4.2}$$

where $\boldsymbol{n}$ is the normal to the boundary $\partial\Omega$ of the domain Ω. From here a discrete formulation of such form is found by first partitioning the domain in N non overlapping elements e, the

domain is then mathematically

$$\Omega = \sum_e \Omega_e \tag{4.3}$$

where the boundary of a given element e defined as the union of all interfaces between all neighboring elements of element e.

$$\partial\Omega_e = \bigcup_f I_f \tag{4.4}$$

The discrete formulation of Eq. (4.2) becomes then

$$\sum_e \int_\Omega \left(\partial_t \boldsymbol{u} - \boldsymbol{S}\right) \varphi dV - \sum_e \left(\int_{\Omega_e} \boldsymbol{F} \partial_x \varphi dV + \sum_{f \in \partial\Omega_e} \varphi \boldsymbol{F} \cdot \boldsymbol{n} dS \right) = 0 \tag{4.5}$$

where the integration over the complete domain is the sum of the integrals over all the elements. Furthermore, similarly to Eq. (4.4), the interface flux term for element e is the sum of the fluxes over the interfaces of the element with its neighbors. The interface term for a given element is defined as

$$\begin{aligned} \sum_{f \in \partial\Omega_e} \boldsymbol{F} \cdot \boldsymbol{n} \varphi dS &= \sum_f \int_f \varphi \boldsymbol{F} \cdot \boldsymbol{n} dS \\ &= \sum_f \int_f \left(\varphi^+ \boldsymbol{F}^+ \cdot \boldsymbol{n}^+ + \varphi^- \boldsymbol{F}^- \cdot \boldsymbol{n}^-\right) dS \end{aligned} \tag{4.6}$$

where by convention the + sign designates the direction of the outward pointing normal to the given interface of element e or in other words $\boldsymbol{n}^+ = \boldsymbol{n}$ and $\boldsymbol{n}^- = \boldsymbol{n}$. However, this expression does not necessarly ensure stability of the method. Instead, the interface flux will not be specified but replaced by an interface flux γ chosen in such a manner as to ensure a stable method for a given application. In practice, this means that γ should be chosen to be consistent or in other words the exact solution should then satisfy the following equation.

$$\sum_e \int_\Omega \left(\partial_t \boldsymbol{u} - \boldsymbol{S}\right) \varphi dV - \sum_e \int_e \boldsymbol{F} \partial_x \varphi dV + \sum_f \int_f \gamma \left(\boldsymbol{u}^+, \boldsymbol{u}^-; \varphi^+, \varphi^-; \boldsymbol{n}\right) dS = 0 \tag{4.7}$$

4.2 Residual equation with the DGM

In the previous section the Galerkin variational formulation Eq. (4.7) was derived and holds true for any $\varphi \in C_1(\Omega)$. One can relate such function to the so called *shape function*. Let's then consider a set of function $\varphi_j \in C^0_\infty(\Omega)$ infinitely continuously differenciable on an element Ω_e and the basis of $C^0_\infty(\Omega_e)$. From there one can show that the Galerkin variational formulation remains valid for such function and thus the formulation becomes the following.

$$\sum_e \int_\Omega \left(\partial_t \boldsymbol{u} - \boldsymbol{S}\right) \varphi_j dV - \sum_e \int_e \boldsymbol{F} \partial_x \varphi_j dV + \sum_f \int_f \gamma \left(\boldsymbol{u}^+, \boldsymbol{u}^-; \varphi_j^+, \varphi_j^-; \boldsymbol{n}\right) dS = 0 \tag{4.8}$$

Since these function are the basis of an element, one can then project $\boldsymbol{u}$,$\boldsymbol{F}$ and $\boldsymbol{S}$ on the basis formed by the *shape function* and approximate such quantities the over the domain Ω.

$$\boldsymbol{u}_h(x) \equiv \sum_{j=1}^N \boldsymbol{u}_j \varphi_j(x) \tag{4.9}$$

$$\boldsymbol{F}_h(x) \equiv \sum_{j=1}^N \boldsymbol{F}_j \varphi_j(x) \tag{4.10}$$

$$\boldsymbol{S}_h(x) \equiv \sum_{j=1}^{N} \boldsymbol{S}_j \varphi_j(x) \tag{4.11}$$

Injecting such expression back in the discretized Galerkin variational formulation Eq. (4.7), the semi-discrete form is obtianed

$$\partial_t \boldsymbol{u}_j = \boldsymbol{M}_{ij}^{-1} \boldsymbol{R}_j \tag{4.12}$$

where $\boldsymbol{R}_j$ is the residual and $\boldsymbol{M}_{ij}$ the mass matrix specific to each element and defined as follows.

$$\boldsymbol{R}_j = \sum \int_e \partial_x \varphi_j \boldsymbol{F}_h dV - \sum_e \int_e \varphi_j \boldsymbol{S}_h dV - \sum_f \int_f \gamma \left(\boldsymbol{u}^+, \boldsymbol{u}^-; \varphi_j^+, \varphi_j^-; \boldsymbol{n} \right) dS \tag{4.13}$$

$$M_{ij} = \int_e \varphi_i \varphi_j dV \tag{4.14}$$

4.3 Hyperbolic system variational formulation

As mentionned previously, the interface flux γ is dependent on the nature of the system at hand. For hyperbolic systems, the interface flux corresponds to convective fluxes. The discretisation of it has been shown to be stabilised with the use of an approximate Riemann solver [16, 34]. The interface flux is then defined as

$$\gamma^c \left(\boldsymbol{u}^+, \boldsymbol{u}^-, \varphi^+, \varphi^-, \boldsymbol{n} \right) = [[\varphi]] \, \mathcal{F}^* \left(\boldsymbol{u}^+, \boldsymbol{u}^-, \boldsymbol{n} \right) \tag{4.15}$$

where $\mathcal{F}^*$ is the numerical flux obtained with the Riemann solver and $[[a]]$ the scalar jump operator defined as $[[a]] = a^+ \boldsymbol{n}^+ + a^- \boldsymbol{n}^-$ with a being a scalar quantity. Such expression can be shown to satisfy all conditions for a stable scheme:

1. **Conservativity:** the system of equations is a set of conservation laws and therefore the discretisation should also describe such principle but a a local level. To ensure conservativity one can impose that the numerical flux is the same of opposite sign at any interface between two elements.

$$\mathcal{F}^* \left(\boldsymbol{u}^+, \boldsymbol{u}^-, \boldsymbol{n} \right) = -\mathcal{F}^* \left(\boldsymbol{u}^-, \boldsymbol{u}^+, -\boldsymbol{n} \right)$$

2. **Consistency:** The residual equation with the exact solution should be zero. This implies then the following.

$$\mathcal{F}^* \left(\boldsymbol{u}, \boldsymbol{u}, \boldsymbol{n} \right) = \boldsymbol{F}^c \cdot \boldsymbol{n}$$

3. **Stability:** the numerical flux should be chosen as to ensure a unique solution.

4.4 Elliptic system variational formulation

The diffusive terms of are discretised using an Internal Penalty Method or IPM. The method is detailled in [34]. In brief, the diffusive interface flux is defined as follows

$$\gamma^d \left(\boldsymbol{u}^+, \boldsymbol{u}^-; \varphi^+, \varphi^-; \boldsymbol{n} \right) = \sigma [[\varphi]] \cdot [[\boldsymbol{u}]] + [[\varphi]] \cdot \{\{\boldsymbol{F}^d\}\} + \theta [[\boldsymbol{u}]] \cdot \{\{\boldsymbol{F}^d\}\} \tag{4.16}$$

where the $\{\{.\}\}$ represent the average operator defined as $\frac{\boldsymbol{a}^+ + \boldsymbol{a}^-}{2}$ for vectors and $[[.]]$ the jump operator previously defined. The σ and θ are arbitrary parameter. The θ parameter value depends on which specific IPM is being used:

- $\theta = 1$, for *symmetric interior penalty* method (SIPDG), in which optimal convergence is observed.
- $\theta = 0$, for *non-symmetric interior penalty* method (NIPDG), which then requires $\sigma > 0$.
- $\theta = -1$, for *incomplete interior penalty* method (IIPDG).

For this work an incomplete interior penalty method was used and thus $\theta = 0$. Lastly, the sigma parameter was studied by [34] and optimal parameter were proposed.

4.5 Application to the plasma equations of this work

In this last section, the above DGM formulation is applied to the equation of this work. The different terms in Eq. (4.1) can be related to the conserved valriables of this work as already shown in the previous chapter in Sec. 3.3. The only missing parameter for the complete defintion of the discretised equatiosn is the numercial flux.

4.5.1 Convective fluxes

The convective flux scheme used in this work is the AUSM+up-AS-cD. This schemes has been developped during the thesis of V. Van der Haegen [26] specifically for plasma flows. As the name suggest, the scheme is a variation of the AUSM scheme adding an all speed handling (in this case for low machs) and a pressure curing term introducing numerical diffusion in the scheme. The crucial part of the scheme for this work is the AS component as the Mach number for electrons is very low.

The AUSM or Advection Upstream Splitting Method is a flux splitting method. In general a fluid contains wavespeed that are define positive and negative, i.e wavespeed propagating downstream and upstream, the basic idea of flux splitting method is then to split these contribution to the convective part of the system. Each component can then be discetised independently. The AUSM flux splits the numerical flux then into a pressure flux and a convective flux.

$$\mathcal{F}^* (\boldsymbol{U})_{L/R} = \mathcal{F}^*{}_c (\boldsymbol{U})_{L/R} + \mathcal{F}^*{}_p (\boldsymbol{U})_{L/R} \tag{4.17}$$

4.5.2 Boundary conditions imposition

The boundary conditions are imposed through ghost cells detailled in [28]. The general imposition is by computing the value of solution at inside the ghost cell such as to ensure that the value at the interface between the ghost cell and the first (or last) cell in the domain is the desired quantity.

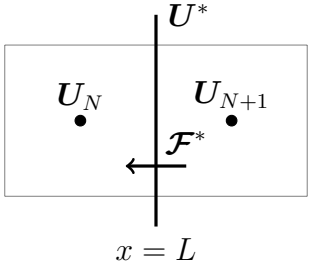

Figure 4.1: Boundary condition schematics at outlet.

Following the convention in Fig. 4.1, the value to be imposed $\boldsymbol{U}^*$ is done by enforcing

$$\boldsymbol{U}^* = \frac{1}{2}\left(\boldsymbol{U}_N + \boldsymbol{U}_{N+1}\right) \quad \Rightarrow \quad \boldsymbol{U}_{N+1} = -\boldsymbol{U}_N + 2\,\boldsymbol{U}^* \tag{4.18}$$

where here $\boldsymbol{U}_{N+1}$ is the ghost cell and $\boldsymbol{U}_N$ the last cell in the domain (outlet in this case).

Chapter 5

Solving strategy

In this chapter, the strategy to solve for the solution of the 1D post-shock relaxation problem is presented. As highligted previously, two solvers are used during the resolution process, one aimed at the CFD part of the problem and the other aimed at computing quantities linked to the chemical properties of the plasma. The strategy can be seen as a parallel solver strategy. The solving procedure is then the following. Starting from initial conditions, the CFD or fluid solver provides to the chemical solver the current state of the solution. The chemical solver then computes all terms related to the chemistry and communicates back the source terms to the fluid solver. With that the fluid solver can solve the system for the current iteration, this process is then repeated for each iteration until the steady-state is reached.

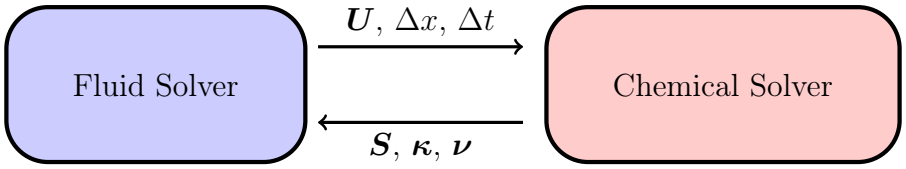

Figure 5.1: Relation between fluid and chemical solver of this work, the fluid solver communicates the solution $\boldsymbol{U}$ while the chemical solver provides source $\boldsymbol{S}$ and chemical properties computations for each species (in particular heat conductivities $\boldsymbol{\kappa}$ and collision frequencies $\boldsymbol{\nu}$).

The computation performed for the chemical solver have arleady been detailed in Chapter 2 of this work, the chemical solver is the MUTATION^{++} library. On the other hand, the fluid solver computation remains to be fully described. In the previous chapter, the discretizaition aspect of the CFD computations was presented. The goal of this chapter is then to present the current resolution scheme implemented in the context of this work.

The 1D post-shock relaxation problem is a steady problem, thus the prefered solver for this work will be a steady-state solver. However, let's remember that one big aspect of this work is to quantify if the sources introduced in Chapter 2 correctly model what is physically occuring at a chemical level. Since, such effects occur at a much smaller time than the fluid time scale, it is useful to define a time accurate scheme to track the evolution of the solution. Such scheme will then allow to have a clearer understanding of the impact of the modeled source terms of this work.

The chapter is then organised as follows. First the steady solver is presented, then the unsteady solver. Firthermore, in the case of the unsteady solver, a stability analysis is performed in order to establish the biggest time step allowed during the integration.

5.1 Steady-state iterative scheme

The steady solver scheme used for this work is the damped Newton-Krylov method using a combination of GMRES and Incomplete LU (or ILU) decomposition as preconditioner. Such method is commonly used when dealing with finite volume methods and has started to be widely adopted for the DGM [30, 34, 39]. The strategy consists in solving the residual system Eq. (**??**) by means of the well known Newton iterative scheme. Contrary to the classical Newton iterator, the linearized system is solved with a Krylov subspace iteration method. Additionally, a pseudo time step is added. The scheme is then the following,

$$\begin{aligned} \partial_t \boldsymbol{U}_j &= \boldsymbol{M}_{ij}^{-1} \boldsymbol{R}_j \\ &\downarrow \\ \frac{\boldsymbol{U}_j^{n+1} - \boldsymbol{U}_j^n}{\Delta\tau^{n+1}} &= \boldsymbol{M}_{ij}^{-1} \boldsymbol{R}_j \end{aligned} \tag{5.1}$$

where $\Delta\tau^n$ is the pseudo time step at the n^{th} iteration. The resolution of the system is then equivalent to solving a pseudo-unsteady problem. In order to maintain a stable scheme, a CFL number should be specified, the pseudo time step is then computed from the given CFL number.

Since the goal here is to reach a steady solution, the pseudo time step should be chosen as big as possible in order to convergence faster. In practice, a common strategy to improve the convergence rate is to adopt an Adaptive CFL strategy. The idea is the following, a initial CFL^0 is provided, such number should be chosen conservatively, i.e not too big as to ensure that the solver can reach the linear regime in the case of strongly non-linear problems. The CFL number at each iteration is then computed in function of the convergence rate and CFL^0. The CFL is then increased inversely proportional to the convergence rate, for this work the definition of the adaptive CFL formula follows [34] and is thus

$$\text{CFL}^n = \text{CFL}^0 \left(\frac{\mathbb{L}_2 \left(\boldsymbol{R}^0 \right)}{\mathbb{L}_2 \left(\boldsymbol{R}^n \right)} \right)^{\alpha} \tag{5.2}$$

where $\mathbb{L}_2$ is the euclidian norm and α is a scalar coefficient, a typical value which has be shown to perform well is 0.7. Moreover, the $\mathbb{L}_2$ norm of the residual is a kin to measure the overall error with respect to the steady-state solution. In general, the n-norm of a vector $\boldsymbol{v}$ is defined as follows.

$$\mathbb{L}_n \left(\boldsymbol{v} \right) = \left(\sum_i |v_i|^n \right)^{\frac{1}{n}} \tag{5.3}$$

However, in practice the most commonly used norms in CFD are the $\mathbb{L}_2$ and the $\mathbb{L}_\infty$, the latter is equal to the biggest absolute value in the vector $\boldsymbol{v}$.

5.2 Time integration scheme

On the other, the time integration scheme for this work is the well known Runge-Kutta 4th order scheme (RK44 or RK4). In general the scheme solves system of the form:

$$\partial_t \boldsymbol{U}_j = f \left(t, \boldsymbol{U}_j \right) \tag{5.4}$$

One can then easily relate such system to the discretized DGM formulation Eq. (**??**) and therefore the f function is then $\boldsymbol{M}_{ij}^{-1} \boldsymbol{R}_j$ in the context of this work. The RK4 scheme then

finds the solution with the following linearizations

$$\begin{aligned} \boldsymbol{U}_j^{n+1} &= \boldsymbol{U}_j^n + \frac{\Delta t}{6}\left(k_1 + 2k_2 + 2k_3 + k_4\right) \\ t^{n+1} &= t^n + \Delta t \end{aligned} \tag{5.5}$$

where t^n is the time of the n^{th} iteration, Δt the time step (here supposed constant for each iterations) and the Runge-Kutta coefficient $K_{i,j}$ are defined as

$$\begin{aligned} k_1 &= f\left(t^n, \boldsymbol{U}_j^n\right) \\ k_2 &= f\left(t^n + \frac{\Delta t}{2}, \boldsymbol{U}_j^n + \frac{\Delta t}{2}k_1\right) \\ k_3 &= f\left(t^n + \frac{\Delta t}{2}, \boldsymbol{U}_j^n + \frac{\Delta t}{2}k_2\right) \\ k_4 &= f\left(t^n + \Delta t, \boldsymbol{U}_j^n + \Delta t\, k_3\right) \end{aligned} \tag{5.6}$$

5.2.1 Stability analysis

One last aspect hat should be addressed, specifically for the RK4 is the domain of stability of the scheme in the constext of the 1D post-shock relaxation problem . Specifically, to ensure the linear stability of the RK4 scheme, the following a Courant–Friedrichs–Lewy or CFL conditions should be respected.

$$\text{CFL} = \sigma\frac{\Delta t}{\Delta x} < 1 \tag{5.7}$$

Here σ is the maximum propagation speed in the system, Δt the time step and Δx the element size. The maximum propagation speed in the 1D post-shock relaxation problem is associated to the electron convective flux matrix eigenvalues, as shown in Sec. 3.3 of this work.

$$\sigma = \lambda_{\max} = |u_e + c_e| \tag{5.8}$$

Furthermore, one can relate Eq. (5.7) to the DGM formulation by expressing Δx in function of the order of interpolation p of each element, the number of element N_x and the length L of the considered domain.

$$\Delta x = \frac{L}{(2p+1)\,N_x} \tag{5.9}$$

Altough the above, relations gives an estimate for Δt, one keep in mind that such conditions does not take into account the influence of the source terms on the stability of the method. Indeed, it has been observed that the source terms have a great impact on the domain of stability. An additional constraint is therefore imposed, the solver should then be able to follow the chemistry, i.e ionization and recombination should be able to be properly captured by the scheme. Mathematically this means that

$$\Delta t \max\left(\nu^E, \nu^I\right) < 1 \tag{5.10}$$

where ν^E and ν^I are the characteristic frequencies for elastic and inelastic sources.
In practice, the evaluation of such frequencies is hard to do, in particular for application such as the 1D post-shock relaxation problem in which these frequencies can take a wide range of values (as they are stongly dependent on the temperature of the system). Under the regimes of temperature of the 1D post-shock relaxation problem , the maximum encountered collision frequency is in the order of 10^{12} Hz . The maximum time step for unsteady simulations for the 1D post-shock relaxation problem with the RK4 scheme should then be

$$\Delta t \sim 10^{-12}\,\text{s}.$$

On the other hand, if only the inelastic terms are considered, the maximum allowed time step jumps to a more favourable value of

$$\Delta t \sim 10^{-8}\,\mathrm{s}.$$

Note that the characteristic frequencies in Eq. (5.10) were obtained specifically in the context of the 1D post-shock relaxation problem regimes of temperatures and densities.

Obviously, the above time steps complexify significantly the practical unsteady resolution of the problem of this work. The stability is then mostly restricted by the second condition. Except if only the convective system is considered, in that case the RK4 scheme is stable with the first condition Eq. (5.7).

Chapter 6

ForDGe solver

The fluid solver used for this work is the ForDGe solver currently being developped at the *Université de Liège*. ForDGe is a high-order cartesian fluid solver using a DG-FEM formulation. Moreover, the solver uses an immersed boundary approach for the mesh discretisation. Such features allows then to tackle coupled physics problems on complex or even moving geometries. The solver is implemented in `C++`.

This chapter is organised in two parts. First, a short description of the ForDGe framework is given. Then, the current work contribution to the solver is presented. For this work, a conservation law class was added with the specific aim to tackle plasma relaxation problems such as the 1D post-shock relaxation problem. The goal here is to provide a brief description of the current capabilities of ForDGe and in particular of the added conservation law.

6.1 Structure and framework

The main class of ForDGe is the `FSolver` class which instantiate the solver parameters from a configuration `json` file. The ForDGe architecture is organised in several modules each treating a specific aspect of the numerical implementation. These modules are then called during the solving procedure by the main class.

For the purpose of this section, only the key modules are presented. Five modules are then considered, handling the generation of the mesh, the definition of the physics of the problem, or in other words the definition of the conservation laws of the problem, the discretization with a DG approach and finally the solving schemes for steady and unsteady problems. Each modules is managed with an overarching class. Since the practical implementations of these classes was not the focus of this work, the presentation here is done to provide a short description of the usage and capabilities of each class. Note also that the descriptions made here reflect the state of ForDGe at the date of the current work. The five classes are then the following:

- `FMesh:` This class implements the mesh generation aspect of the solver. The class allows to generate cartesian meshes in all three spatial dimension with a user specified order of interpolation for each element in the mesh. All relevant informations are then stored for each element in a dedicated data structure for ease of access in other classes.

- `FConservationLaw:` The conservation law module implements the physics of the problem to be solved. The base class acts a factory or virtual class allowing then the user to implement its own conservation law class for the desired physics. The user should then specify the relevant scales of the problem, the appropriate flux schemes, the computation of the sources, the implementation for the boundary conditions enforcement, the initialization

of the solution with initial conditions and lastly the implementation of post-processing functions to compute relevant physical quantities (such as pressure, temperature, etc). At current stage of development, several conservation laws have been implemented giving future developers a basis for proper implementation of their own conservation law class.

- `FDGBase`: This class implements the disretization module of FORDGE . The module consist into the evaluation of the residual from each of its contribution through the DG formulation discretization. The discretization modules allows then to treat the DG discretization independently from the physics of the problem.

- `FIterator`: The iterator class implements the Newton-Krylov iterator solvers for steady-state problem. Additionally, the class provides several strategies to deal with diverse problems, such as adaptive CFL to improve the convergence rate.

- `FTimeIntegration`: Similar to the previous class, this class provides an interface to solve unsteady problem by providing several time accurate integration schemes. The current implemented schemes are based on the well known Runge-Kutta methods. These schemes can be spit in explicit schemes (RK44 or Runge-Kutta 4th order) and implicit schemes (RORK, ESDIRK64[1]) allowing great flexibility when dealing with unsteady problems.

6.2 Conservation class for plasma relaxation test cases

The added conservation law class for this work is the `FPlasmaRelaxationCLaw` class. This class solves for problems in which the physics is determined by conservation systems of the form of the system of equations introduced in Chapter 1. In particular, the class implementation was done in order to solve the 1D post-shock relaxation problem . However, the class also allows to tackle other similar test cases. To do so, the user can specify several optional parameters allowing to modify the governing equations, the chemistry and its related source terms but also all other aspects relevant to the discretization process (flux scheme, boundary condition enforcement, etc). In this section, the main options provided by the `FPlasmaRelaxationCLaw` are presented.

The first option is the formulation of the equations to be solved, which is specified with the `Model` parameter. In brief, this options introduces different systems of conservation equations based on the system developed in this work Eqs. (1.10–1.12). Currently three models are possible:

- The default model, which simply solves the system Eqs. (1.10–1.12) and is referred with the `FullCoupling` keyword.

- A modified source model, the `MassCoupling` model. Here the source terms are modified for the momentum and total energy equations. The system becomes then the following, where the modified terms with respect to the default model are highlighted in red.

$$\begin{aligned} \partial_t n_\alpha + \partial_x \left(n_\alpha u_\alpha\right) &= \dot{\omega}_\alpha^{(n)} \\ \partial_t \left(n_\alpha u_\alpha\right) + \partial_x \left(n_\alpha u_\alpha^2 + \frac{p_\alpha}{m_\alpha}\right) &= u_\alpha \dot{\omega}_\alpha^{(n)} \\ \partial_t \left(n_\alpha E_\alpha\right) + \partial_x \left(n_\alpha H_\alpha u_\alpha\right) &= -\frac{1}{m_\alpha}\partial_x q_\alpha + E_\alpha \dot{\omega}_\alpha^{(n)} \end{aligned} \tag{6.1}$$

[1]These schemes will not be detailled in the present work as they were not used for this work. The goal here is just to mention the different possibilities of the FORDGE solver.

- The last model is the `Euler` model, which as the name suggest solves the Euler equations and can be used to study the system in a decoupled form.

$$\begin{aligned} \partial_t n_\alpha + \partial_x \left(n_\alpha u_\alpha \right) &= 0 \\ \partial_t \left(n_\alpha u_\alpha \right) + \partial_x \left(n_\alpha u_\alpha^2 + \frac{p_\alpha}{m_\alpha} \right) &= 0 \\ \partial_t \left(n_\alpha E_\alpha \right) + \partial_x \left(n_\alpha H_\alpha u_\alpha \right) &= 0 \end{aligned} \tag{6.2}$$

Additionally to the `Model` option, sources terms options are available and allow to specify the computation and type for these terms. Note that by default the source terms are computed as described in Chapter 2 of this work with the help of the MUTATION^{++} library.
The `SourceComputation` option can take either the `Mutation` or `Hardcode` arguments. These argument indicate which algorithm is used to compute the source terms. Indeed, computations with MUTATION^{++} have shown to be somewhat expensive and thus the user might want to compute source term with an hardcoded alogrithm. Currently, the hardcoded algorithm follows the development of Chapter 2 of this work and only is available for the Agon 3 mixture model. The second option is the `SourceType`, which allows the user to add only `Inelastic` or `Elastic` contributions to the source terms. The user can then assess the influence of each contribtuion separately. By default both contributions are taken into account, the default mode is referred with the `All` keyword.

Regarding the chemistry, one should encode a mixture (and mechanism) file in MUTATION^{++} and then indicate to the `FPlasmaRelaxationCLaw` class the name of such file under the `Mixture` option. As stated before, currently only the Argon 3 mixture is supported and is referred with the `argon_3` keyword. The class is then built in order that future users can specify their own mixtures, provided that a proper source modeling is done. Additionally, in order to ensure that a `Hardcode` computation can be done, the user needs to provide Arrhenius law parameters for each foward and backward reaction of the new mixture.

Until now, all presented parameters are optional since a default value overrides in case no value is specified by the user. However, some options should be specified as they depend on the considered test case. These parameters are the scaling parameters defined in Sec. 3.2, in particular the reference scales for particle density and temperature. These scales should be specified with the `ReferenceNumberDensity` and `ReferenceTemperature` parameters. Moreover, one should also be aware that minimum quantities are defined in the class for specific physical quantities. Indeed, negative densities or temperatures are not physical and should be avoided. Therefore, the minimum quantities for particle density and temperature are chosen respectively as $10^{-40}\,\mathrm{m}^{-3}$ and $100\,\mathrm{K}$. Note these values are chosen for plasma applications where wide variation of particle densities are possible and low temperature such as $100\,\mathrm{K}$ rarely occur.

The previous described options are specific to the `FPlasmaRelaxationCLaw` class. The rest of the options tend to be common to each conservation law class in FORDGE . These options allow the user for instance to specify the flux scheme, the type of initial and boundary conditions and the post processing options. Let's then describe the current variations of each of these parameters for `FPlasmaRelaxationCLaw` class.
Currently, four flux schemes are available: the `LaxFriedrichs` scheme [**Lax**], an entropy stable `Roe` scheme [27] applied to the system of Eqs. (1.10–1.12) and lastly the `AUSM+` and `AUSM+UpAScD` schemes both described in Appendix. **??**.

Furthemore, the class allows to specify either uniform conditions in the one dimensional case with the `Uniform1D` or `Custom` conditions. For the uniform case, the user should then specify the following parameters:

- `NumberParticle:` The plasma overall mixture particle density in m^{-3}.
- `DegreeOfIonization:` The ratio Z of charged number particles to overall number particle in the plasma mixture.
- `Velocity:` The velocity of the plasma mixture in m/s, each species velocity is then supposed to be the same as the plasma velocity.
- `ElectronTemperature:` The temperature of electrons or the vibrational temperature of the plasma in K.
- `HeavyTemperature:` The common heavy temperature in K.

From here, the class initializes the solution to be constant everywhere with the following values. The particles densities are

$$\begin{aligned} &\text{for neutrals} && n_\alpha(x,0) = \frac{(1-Z)\,n}{(N_{\mathcal{S}} - N_Z)} \\ &\text{for ions and electrons} && n_\alpha(x,0) = \frac{Zn}{N_Z} \end{aligned}$$

where n is the value specified with the `NumberParticle` parameter and N_Z, $N_{\mathcal{S}}$ respectively the number of charged species and the number of species in the mixture. Momentum and total energy are then computed from their relations to speed, temperature and particle density.

Regarding, boundary conditions, three type are implemented. First, `SubsonicInlet` and `SubsonicOutlet` conditions which refer to the boundary conditions described in the previous chapters of this work. One should then specify all quantities at the inlet and the pressure at the outlet with dimensional units. The user can then define the type of inlet with the `InletType` parameter, the allowed type are summarised in Table. 3.3. However, the outlet can currently only be a pressure subsonic outlet boundary.
The third available boundary conditions is a `Wall` boundary conditions. The implementation enforces then a no penetration and no slip condition, i.e all component of each species velocity are enforced to be zero, and a zero heat flux Neumann condition, i.e $\partial_x T = 0$.

Lastly, several physical quantities, other than the conserved variables, can be exported during the soling procedure. The quantities of interest here are the temperature, the pressure, the velocity and the mass density of each species. Moreover, each source term can also be export with the `DensitySourceTerm`, `MomentumSourceTerm` and `EnergySourceTerm` keywords.

Part III

Results

Chapter 7

Preliminary test cases

Solving problems such as the 1D post-shock relaxation problem can be a difficult task as many aspects of the discretisation can fail. Therefore, to be able to assess the correct implementation of the numerical methodology presented previously, preliminary test cases are done. These test cases are specifically designed to validate each part of the discretisation. Two test cases are then selected, the first dedicated to the convective part of the system and the second to the sources.

7.1 The 1D step propagation test case

This test case is aimed at studying the propagation of a discontinuity in the domain. Specifically, the solution is initialized with a density step in the middle of the domain. Moreover, the plasma is assumed to be at rest, i.e no velocity, and all species share a common temperature. This is then practical to easily identify different behaviour between each species

In the absence of sources and without heat flux, the system of equations becomes the multi-species Euler 1D system and is thus

$$\begin{aligned} \partial_t n_\alpha + \partial_x \left(n_\alpha u_\alpha\right) &= 0 \\ \partial_t \left(n_\alpha u_\alpha\right) + \partial_x \left(n_\alpha u_\alpha^2 + \frac{p_\alpha}{m_\alpha}\right) &= 0 \\ \partial_t \left(n_\alpha E_\alpha\right) + \partial_x \left(n_\alpha H_\alpha u_\alpha\right) &= 0 \end{aligned} \tag{7.1}$$

where each convective system associated to each particle is independent from each other. The system is said to be decoupled. To initialize the solution some reference quantities are first taken. A temperature $T_0 = 300\,\mathrm{K}$ and a pressure $p_0 = 685.28$, the plasma composition is then equally distributed between each species. The system is then solved with the time integration RK4 scheme. Having chosen a low temperature profile is then useful as a more generous time step can be define (remember that the time step for RK4 is dependent on the speed of sound of electrons, itself dependent on temperature). For this test case, the time step is then $10^{-8}\,\mathrm{s}$.

The results of this test case are displayed in Fig. 7.1 for particle density, Fig. 7.2 for speed and Fig. 7.3 for pressure. All quantities are displayed with non-dimensional units. As expected, one can notice that the convection part of the discretization is properly treated. Indeed, when perturbing a fluid at rest, one should expect waves to ripple from the origin of the perturbation. Furthermore, notice that the electron dynamics are much faster than heavy species. From the figure on can measure the propagation speed of the density waves. The electrons propagation speed is then $\sim 7.92 \times 10^4\,\mathrm{m/s}$ and $\sim 297\,\mathrm{m/s}$ for heavy species. Since the fluid is at rest, these

measurements correspond to the speed of sound of each species. One can compare such value with the speed of sound expression Eq. (1.18). Doing so, the speeds of sound at $T = 300\,\mathrm{K}$ are then $8.7051 \times 10^4\,\mathrm{m/s}$ and $322.6\,\mathrm{m/s}$ respectively for electrons and heavy species. One can then conclude that the measurements match the expected physics.

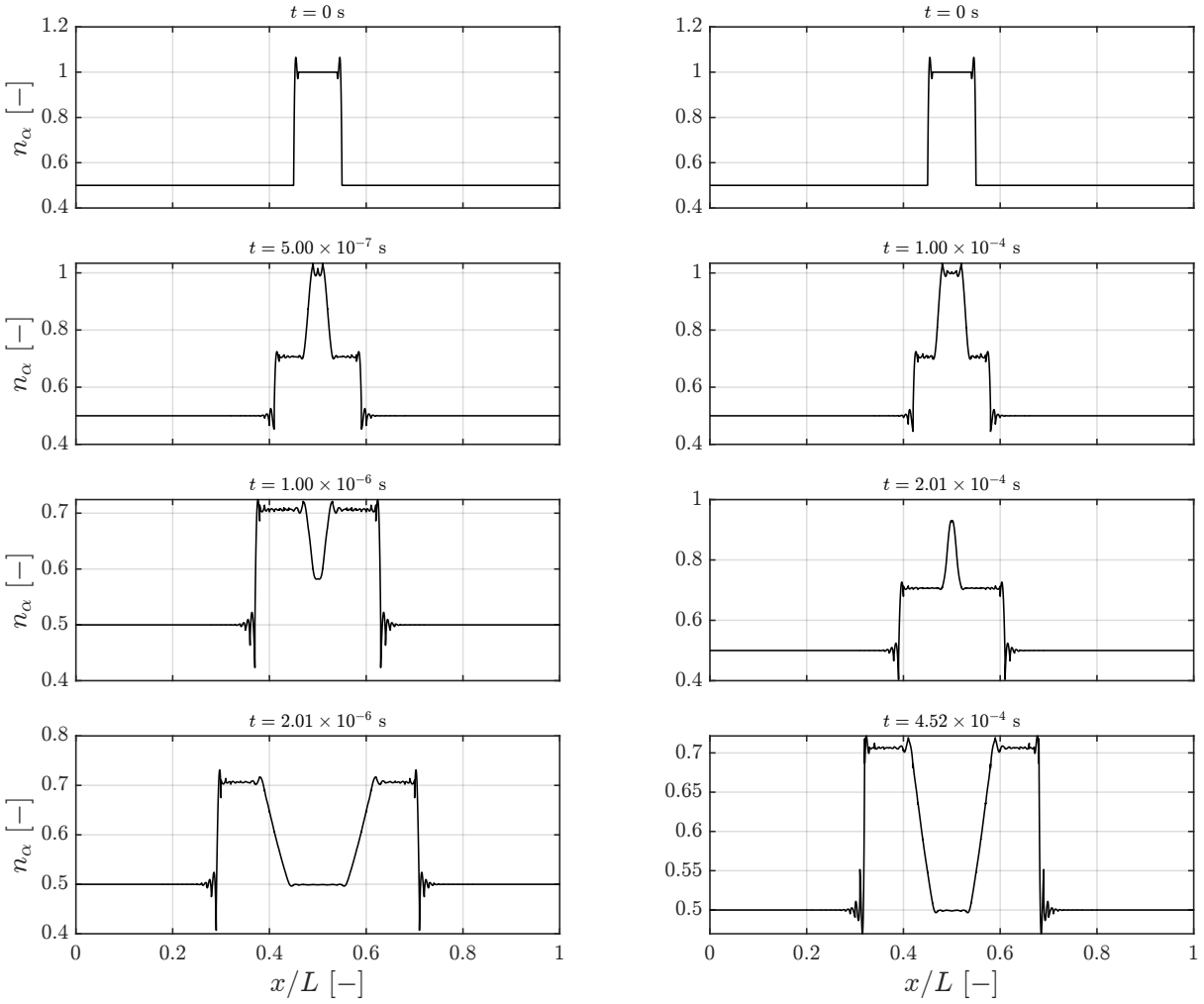

Figure 7.1: Non-dimensional particle density resulting from initial density step perturbation with no coupling between the species of the plasma, left for electrons and right for heavy species.

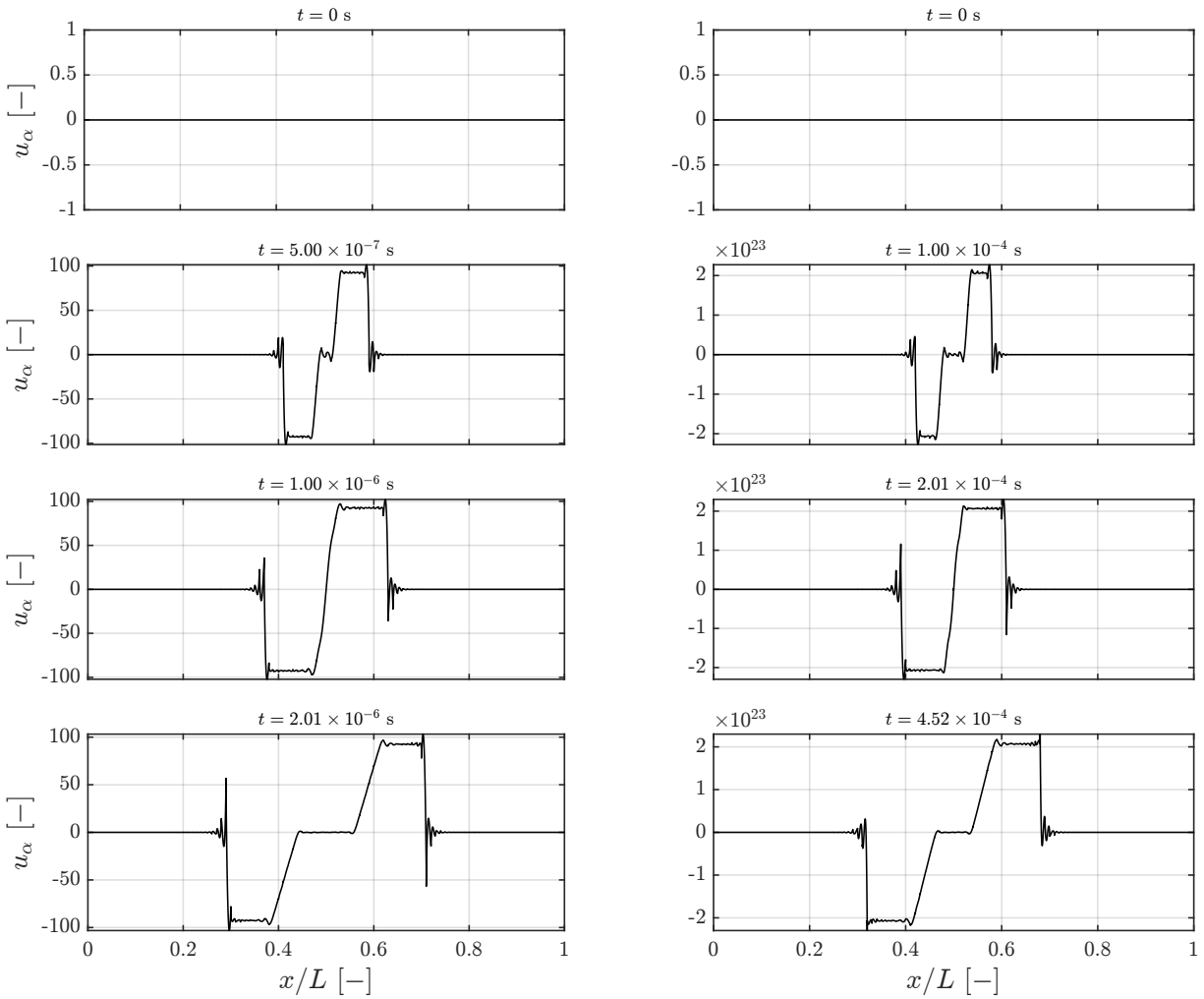

Figure 7.2: Non-dimensional velocity resulting from initial density step perturbation with no coupling between the species of the plasma, left for electrons and right for heavy species.

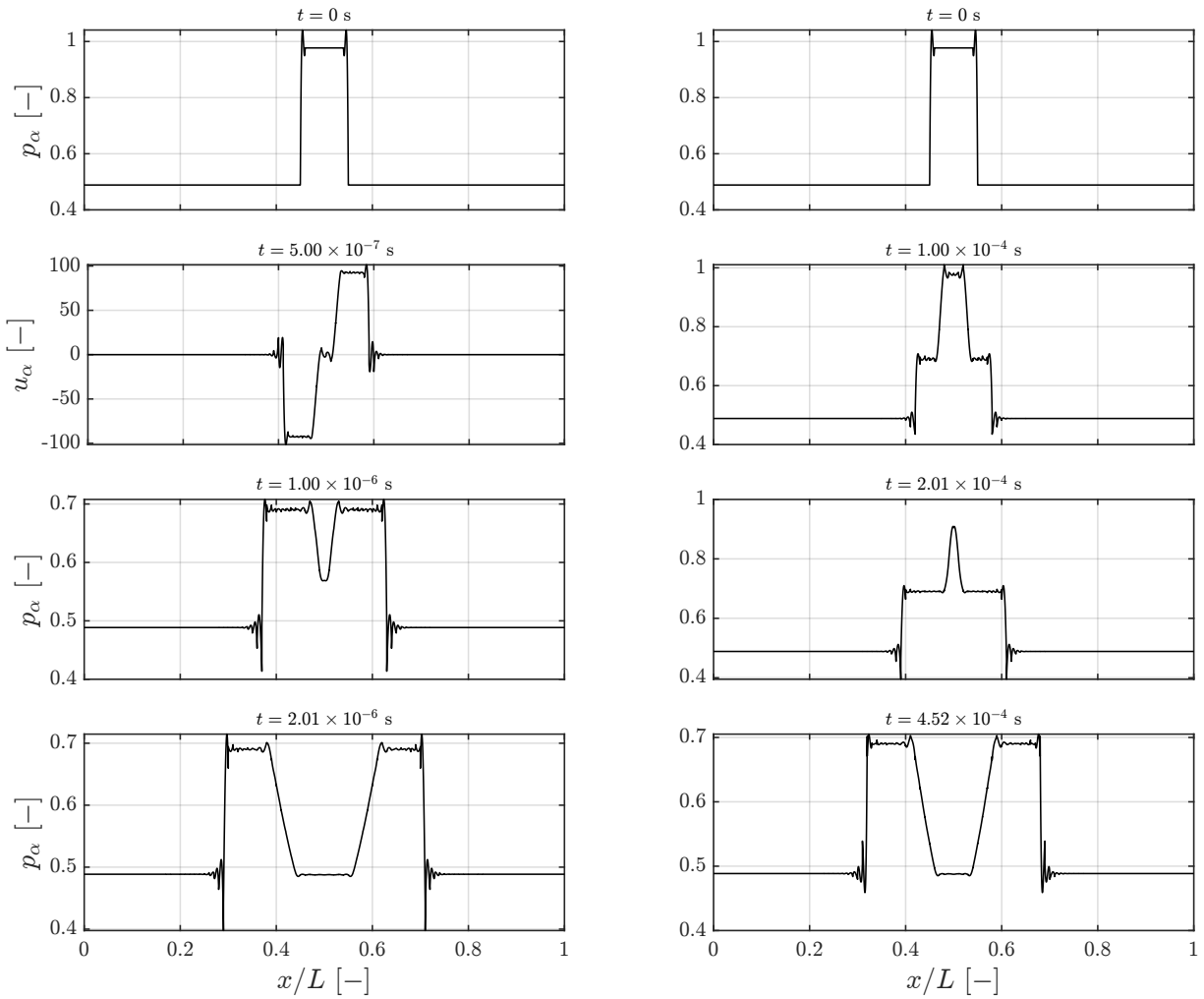

Figure 7.3: Non-dimensional pressure resulting from initial density step perturbation with no coupling between the species of the plasma, left for electrons and right for heavy species.

7.2 The argon reactor test case

This test case is aimed at testing the source implementation. For this purpose, the test case describes the evolution of a system in a non-equilibrium state towards and equilibrium point. For this case, the non-equilibrium conditions are the ones described in the 1D post-shock relaxation problem right after the shock. However, specifically for this case, the fluid is at rest. The system should then evolve towards the equilibrium solution of the 1D post-shock relaxation problem mainly through chemical exchanges.

The solution is initialized with uniform conditions and wall boundary conditions are enforced (no slip, no pen). Moreover, the same scaling of Sec. 3.2 is used here. Lastly, the solution is solved with the time integration RK4 scheme detailed previously in Chapter 5. Since only inelastic terms are present here, the time step for the time integration is set to $\Delta t = 10^{-8}$. The system of equations to be solved is the following.

$$\begin{aligned} \partial_t n_\alpha + \partial_x \left(n_\alpha u_\alpha \right) &= \dot{\omega}_\alpha^{(n)} \\ \partial_t \left(n_\alpha u_\alpha \right) + \partial_x \left(n_\alpha u_\alpha^2 + \frac{p_\alpha}{m_\alpha} \right) &= \dot{\omega}_\alpha^{(m)} \\ \partial_t \left(n_\alpha E_\alpha \right) + \partial_x \left(n_\alpha H_\alpha u_\alpha \right) &= \dot{\omega}_\alpha^{(e)} \end{aligned} \tag{7.2}$$

The solutions is then displayed in Fig. 7.4. To be specific, the quantity displayed in each figure is the evolution of the average of said quantity over the domain. Since uniform conditions are provided and the production is uniform over the domain, the solution and its average are the same.

Regarding the results, several observations can be made. First, a mass equilibrium was properly achieved. One can verify this, as the density production $\dot{\omega}^{(n)}$ in Fig. 7.4c eventually reaches zero and no mass exchange is then possible between each species.
Furthermore, the fluid remains at rest as expected (Fig. 7.4e). Additionally, it is observed that the velocity is not exactly zero and some very small variations appear. This variations are negligible, yet one can notice that the species mostly impacted by it are the electrons.

On the other hand, some unexpected behaviours can be observed. In particular regarding the temperature evolution. Indeed, it seems that inelastic terms do not exchange temperature. However, one can notice in Fig. 7.4d that the inelastic energy production is not zero but still does not seem to impact the temperature. One possible explanation could be the chosen scaling. Indeed, the scaling of the energy is species dependent but the source

Lastly, the equilibrium ionization fraction can be compared to the one from the 1D post-shock relaxation problem . This is done as a validation step even if the observations about temperature imply that the ionization rate should differ. Indeed, the rate from the 1D post-shock relaxation problem is $\alpha = 0.0679$ while the rate of this solution is $\alpha = 0.0301$.

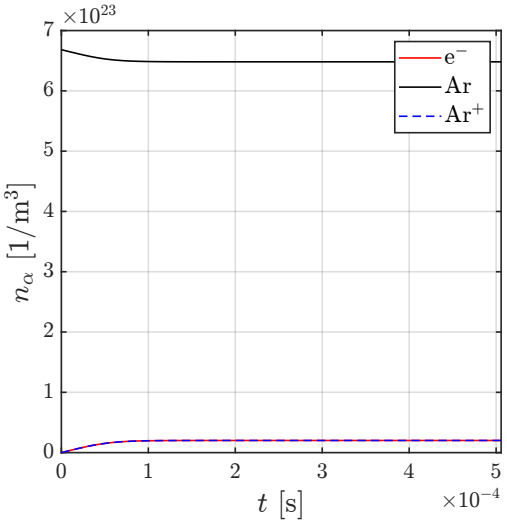

(a) Particle density evolution.

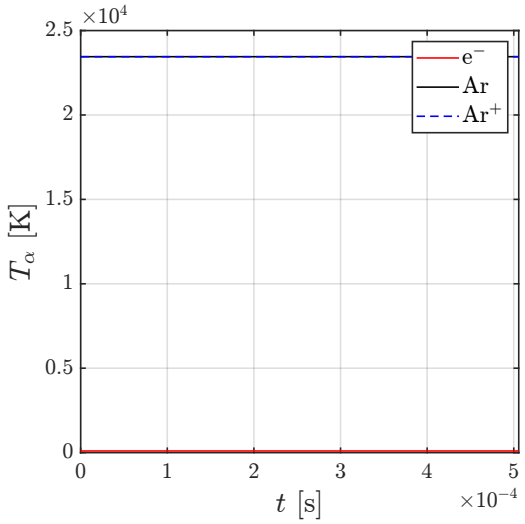

(b) Temperature evolution.

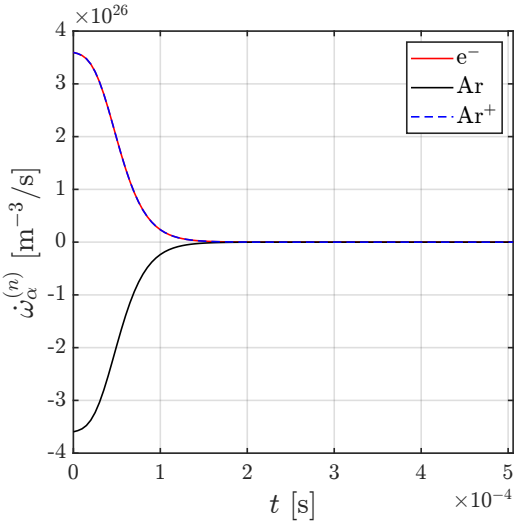

(c) Density production evolution.

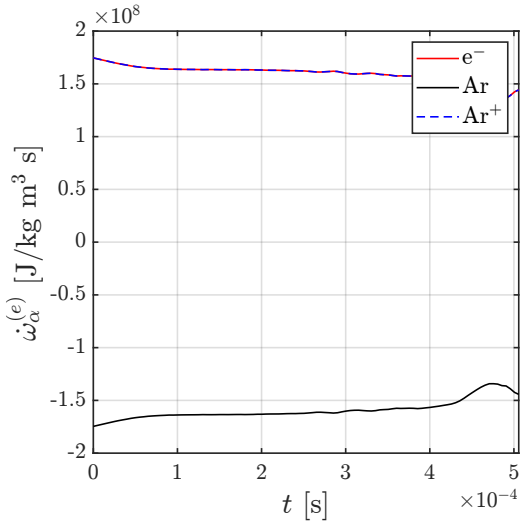

(d) Energy production evolution.

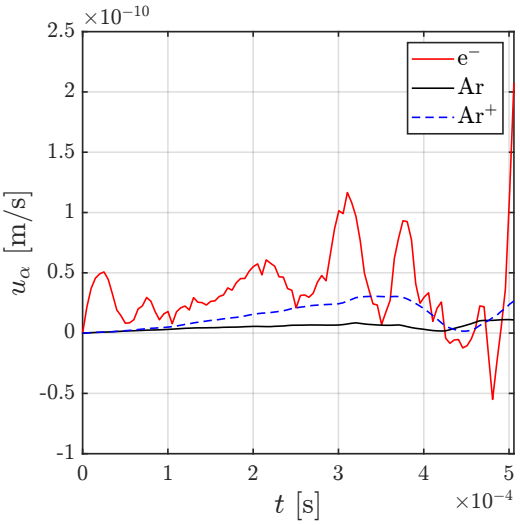

(e) Velocity evolution.

Figure 7.4: Equilibrium solution for the ionization process of argon gas at rest.

Chapter 8

The 1D post-shock relaxation problem

In this last chapter, the current solution of the 1D post-shock relaxation problem is presented. As one will notice, the results presented here are not conclusive in the sense that the expected solution as not been obtained. Therefore, this chapter aims to present the different simulations done in the context of this work and determine the most sensitive parameters. The results here are obtained with the steady solver. Sadly, because of time constraints unsteady simulations could not be done realistically such as to show interesting results.

8.1 Steady-state results

Several simulations were done by varying the boundary conditions and initial CFL number. The presentation here will compare the differences observed in between each setup. In each case, the solution is compared to the reference solution shown in Chapter 3 of this work. Furthermore, irespectively of the chosen setup the range of acceptable initial CFL numbers was observed to be

$$10^{-7} < \mathrm{CFL}^0 < 10^{-4}.$$

Simulations with values of CFL^0 outside of this range would then diverge after a few iterations. Lastly, for all simulations the minimum relative convergence was set to 10^{-8}.

The solution obtained are then shown in Fig. 8.1 and Fig. 8.2 with respectively a density and pressure inlet boundary type conditions as highlighted in Sec. 4.5.2. For both case the following observation can be made:

- The solution equilibrium state is not maintained in the equilibrium region (zone V), in particular the temperatures start diverging from one another and are practically never exactly equal.
- A density overshoot appear at roughly $x/L \sim 0.4$.
- The electrons particle density seems is a linear.

These observations can partially be explained from the fact that the result presented here are not strictly the results of the converged steady solution. Indeed, the convergence rate is quite slow and did not reach the selected minimum relative convergence. The convergence for the second simulation can be seen on Fig. 8.3. This sadly, could have potentially be fixed, but a lack of time and a slow convergence rate did not allowed for longer computations. This mean that the pseudo-transient term is still active in the residual and thus could explain for instance the appearance of overshoots.

Overall, from these two simulation, the second seems to be more consistent with the expected solution. Indeed one can observe that contrary to the first one, the temperature profiles seem to be maintained at the correct values near the boundaries while in the first simulation the heavy temperature is observed increasing at the inlet.
The rest of this chapter focus then on the different results for the second simulation, i.e the solution with a pressure inlet type boundary. The current solution is then showcased in Fig. 8.2, the velocity of the mixture in Fig. 8.4 and the source terms and in particular the energy source in Fig. 8.5.

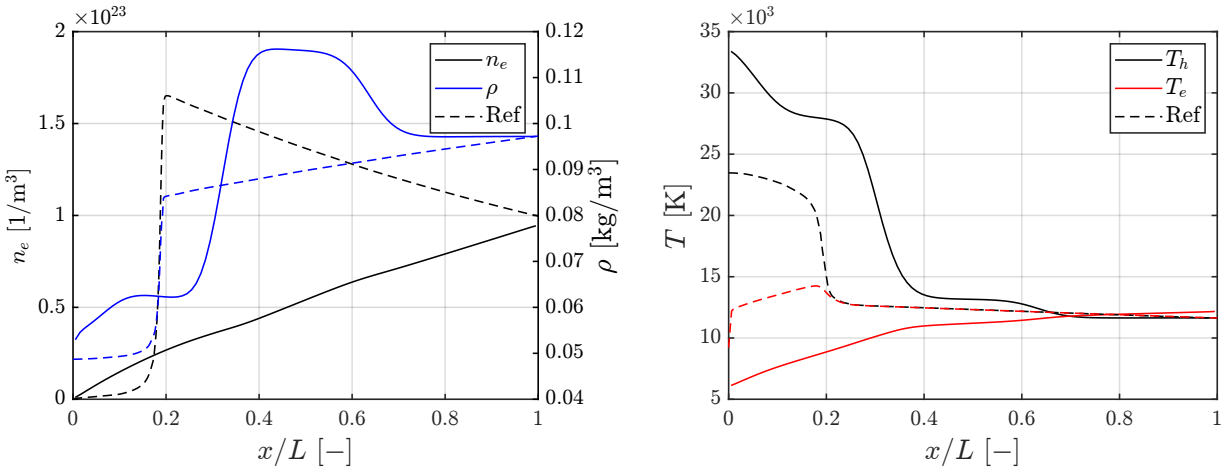

(a) Plasma density and electron particle density.

(b) Temperatures.

Figure 8.1: Solution with $\text{CFL}^0 = 10^{-6}$ and density inlet type boundary conditions as detailed in Sec. 4.5.2

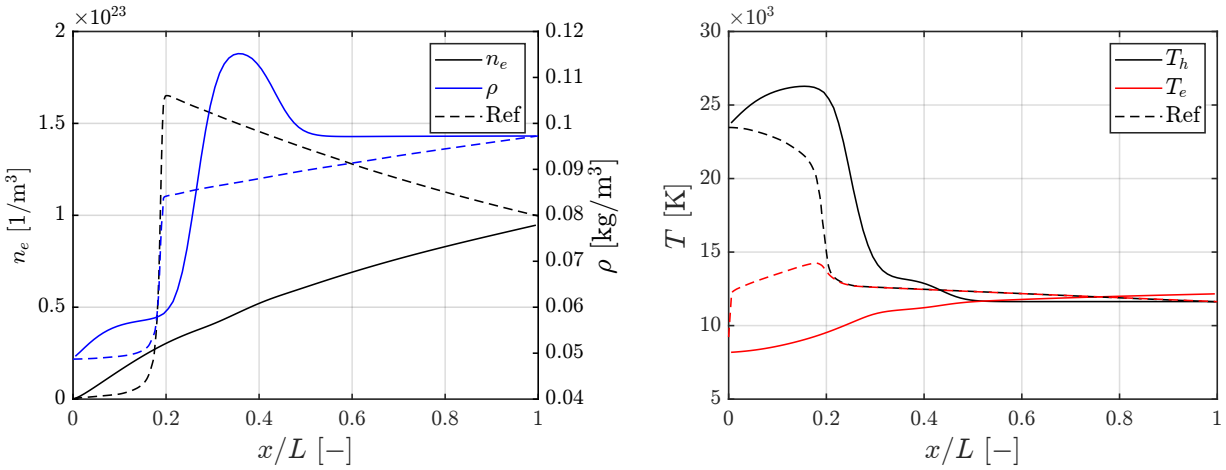

(a) Plasma density and electron particle density.

(b) Temperatures.

Figure 8.2: Solution with $\text{CFL}^0 = 10^{-5}$ and pressure inlet type boundary conditions as detailed in Sec. 4.5.2

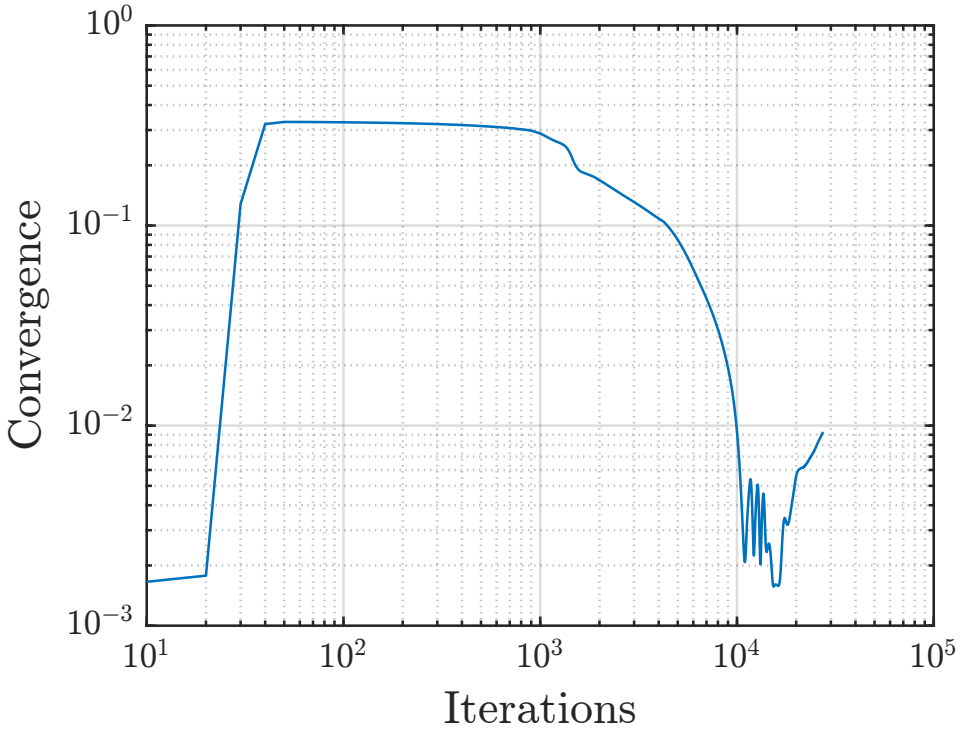

Figure 8.3: Convergence rate with $\text{CFL}^0 = 10^{-5}$ for pressure inlet type boundary condition.

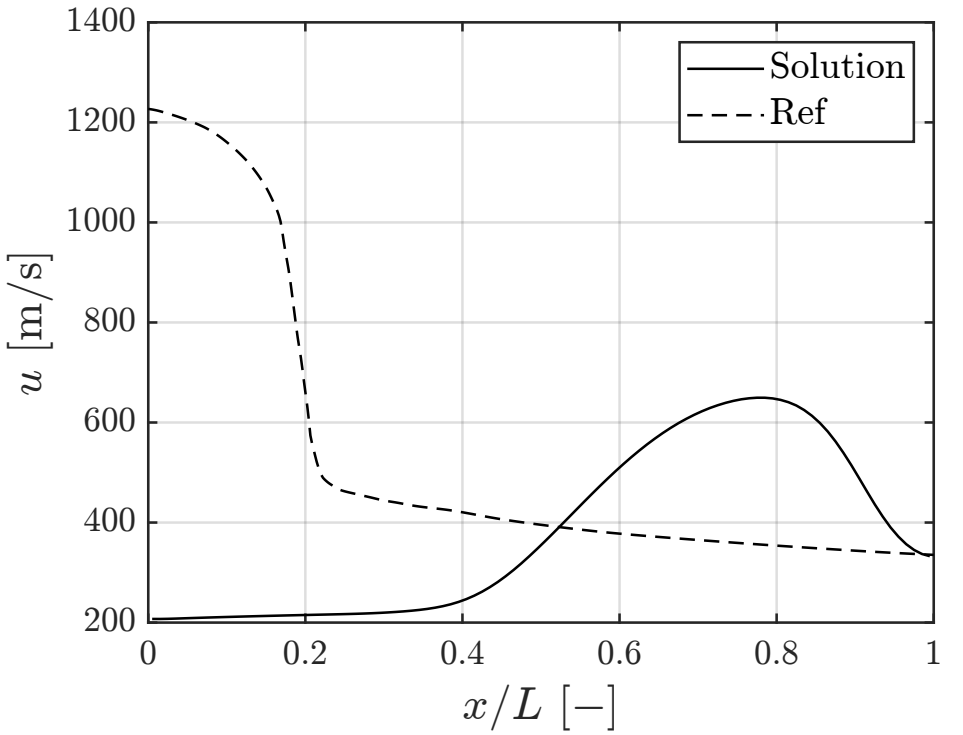

Figure 8.4: Comparison of velocity with $\text{CFL}^0 = 10^{-5}$ for pressure inlet type boundary condition.

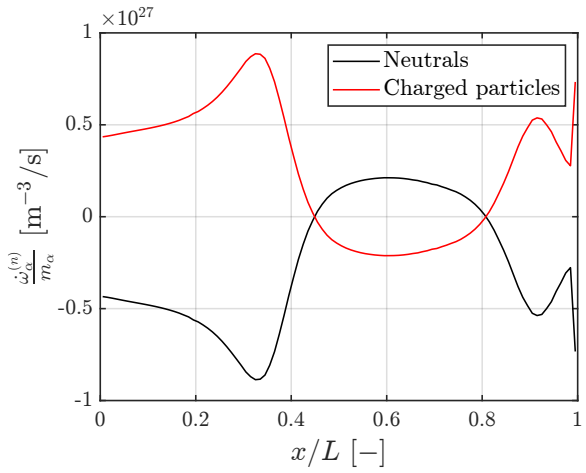

(a) Particle density production.

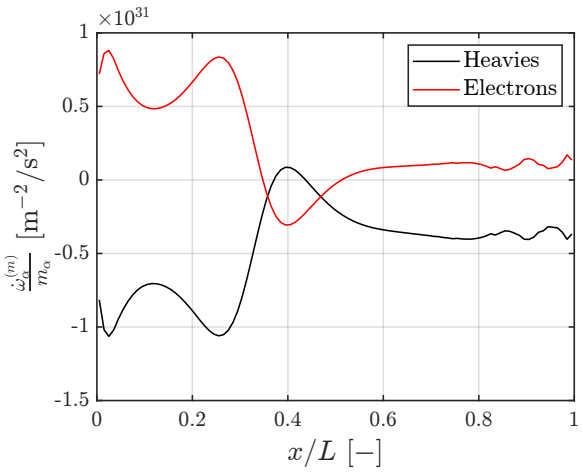

(b) Momentum production.

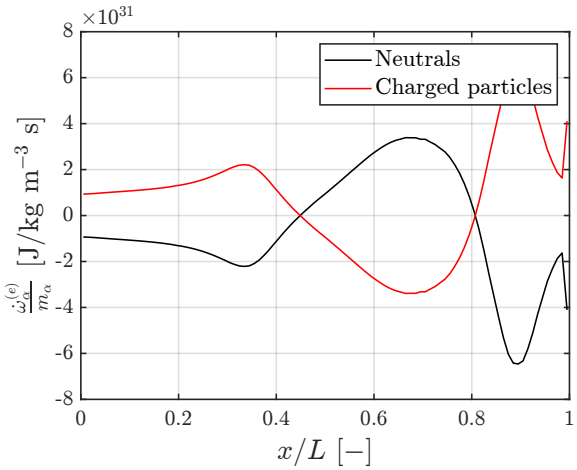

(c) Energy production.

Figure 8.5: Source terms with $\text{CFL}^0 = 10^{-5}$ and pressure inlet type boundary conditions.

Conclusion and future work

In this work, a numerical methodology to resolve reactive plasma flow problems has been developed. First the physics of such flow was studied and characterised with a set of governing laws under a Multi-fluid formulation. Additionally, the resolution of these governing laws was shown to be dependent on the chemistry of the plasma and thus a chemical and source model was developed according to the problem of this work. Regarding the problem of interest, the 1D post-shock relaxation problem was properly introduced and formally defined from [31, 46].

In the second part of this work a working DG-FEM formulation was applied to the governing equation of this work. Steady and unsteady scheme were then introduced to solve the 1D post-shock relaxation problem . Lastly, the implementation of the numerical methodology was done in the FORDGE solver by introducing a dedicated conservation law class, the `FPlasmaRelaxationCLaw` . Currently, the class handles chemical interactions with the Argon 3 model introduced in this work. Hovewer, the class provides tools to handle other collisional chemical model for reactive plasma flows.

In the last part of this work, the results achieved with the numerical method of this work was presented. Additionally to the problem of this work, two other test cases were explored in a quest to assess the correct implementation of each individual part of the discretization process. From here several observations were made:

- The propagation of an acoustic perturbation is correctly handled by the discretization.
- The inelastic contibution to the energy source term is inacurate, as it fails to properly describe the physical exchange of temperature in between electrons and heavy species.
- The current source model does not maintain the equilibrium state in zone V of the 1D post-shock relaxation problem , as temperature profiles diverge.

To conclude, the current work although not successful in solving the 1D post-shock relaxation problem , this work has layed ground for future studies. The main culprit seems to be the source model, in particular regarding temperature exchanges. Indeed, even if the methodology did not result in the desired solution, this work results can be used to establish guidelines on future developments in order to develop a robust numerical method for tackling problems of the type of the 1D post-shock relaxation problem . Here, two directions are suggested:

- First one could integrate a more complex source model to develop in particular the exchange of temperature due to chemical reaction, one example is the work of Benilov [6] were collision integrals are fully described for the Multi-fluid model.
- Regarding the set up of the problem, one option that was not explored in this work is to include the shock in the the numerical domain. The resolution is a bit different as shock capturing method need to be developed. Furthermore, such resolution should be done in time accurate simulation which can be quite expensive. On the other hand such approach is quite common and tends to be preferred, one example is for instance [7].

Appendices

Appendix A

Rankine-Hugoniot relations

In this appendix the rankine-hugoniot are briefly sumarised. The Rankine-Hugoniot relations also referred to as Rankine–Hugoniot jump conditions describe the relations of the state left and right of a shock wave. For this work, the focus is specifically on the normal and steady shock relations. The Rankine–Hugoniot conditions can be expressed then as

$$\begin{aligned} \rho_1 u_1 &= \rho_2 u_2 \\ \rho_1 u_1^2 + p_1 &= \rho_2 u_2^2 + p_2 \\ h_1 + \frac{1}{2} u_1^2 &= h_2 + \frac{1}{2} u_2^2 \end{aligned} \tag{A.1}$$

which in short describe the conservation of mass, momentum and energy through the shock.

Furthermore, one can expand such relations if perfect gas are considered by introducing the perfect gas law relation. One can then express the ratio of a conserved variable left to right (assuming that the left mach number is supersonic) as follows.

$$\begin{aligned} M_2^2 &= \frac{1 + \frac{\gamma-1}{2} M_1^2}{\gamma M_1^2 - \frac{\gamma-1}{2}} \\ \frac{\rho_2}{\rho_1} &= \frac{(\gamma+1) M_1^2}{2 + (\gamma-1) M_1^2} \\ \frac{p_2}{p_1} &= 1 + \frac{2\gamma}{\gamma+1} \left(M_1^2 - 1 \right) \\ \frac{T_2}{T_1} &= \frac{p_2/p_1}{\rho_2/\rho_1} \end{aligned} \tag{A.2}$$

Appendix B

Characteristic analysis of the 1D Euler equations

This appendix treats the analysis of the characteristic for the Euler system in the one dimensional case. It follows the analyis as detailed in the book of C. Hirsch [28].
First, the methodology to determine the characteristic variables of the Euler system is described, by extension this methodology is valid for any similar system. Then the characteristic analysis of the Euler system is done and examples of typical boundary conditions are given.

B.1 Characteristic variables

The one dimensional Euler system can be written in matrix form as follows.

$$\partial_t \boldsymbol{U} + \partial_x \boldsymbol{F} = 0 \tag{B.1}$$

where the conserved variable $\boldsymbol{U}$ and the fluxes $\boldsymbol{F}$ are

$$\boldsymbol{U} = \begin{bmatrix} \rho \\ \rho u \\ \rho E \end{bmatrix} \quad \boldsymbol{F} = \begin{bmatrix} \rho u \\ \rho u^2 + p \\ \rho u H \end{bmatrix}.$$

One can then introduce the flux jacobian matrix $\boldsymbol{A} = \frac{\partial \boldsymbol{F}}{\partial \boldsymbol{U}}$.

$$\boldsymbol{A} = \begin{bmatrix} 0 & 1 & 0 \\ \frac{1}{2}(\gamma-3)u^2 & (3-\gamma)u & \gamma-1 \\ -\gamma E u + (\gamma-1)u^3 & \gamma E - \frac{3}{2}(\gamma-1)u^2 & \gamma u \end{bmatrix}$$

and the system Eq. (B.1) can be rewritten in functin of partial derivative of the conserved variables $\boldsymbol{U}$

$$\partial_t \boldsymbol{U} + \boldsymbol{A}\partial_x \boldsymbol{U} = 0 \tag{B.2}$$

The eigenvalues of the flux jacobian matrix describe the propagation speed of the waves associated to each characteristic. To determine the eigenvalues it is often easier to proceed under a primitive variable formulation, let's define $\boldsymbol{V}$ as the primitive variable vectors. With a particular choice of primitive variable one can define the transformation matrix $\boldsymbol{M}$ from primitive to conservative variables.

$$\boldsymbol{M} = \frac{\partial \boldsymbol{U}}{\partial \boldsymbol{V}} \tag{B.3}$$

Similarly to the conservative system formulation, a primitive variable formulation is found with the transformation matrix $\boldsymbol{M}$.

$$\begin{aligned} \boldsymbol{M}\partial_t \boldsymbol{V} + \boldsymbol{A}\boldsymbol{M}\partial_x \boldsymbol{V} &= 0 \\ \boldsymbol{M}^{-1} \cdot (\boldsymbol{M}\partial_t \boldsymbol{V} + \boldsymbol{A}\boldsymbol{M}\partial_x \boldsymbol{V}) &= 0 \\ \partial_t \boldsymbol{V} + \underbrace{\boldsymbol{M}^{-1}\boldsymbol{A}\boldsymbol{M}}_{=\tilde{\boldsymbol{A}}}\partial_x \boldsymbol{V} &= 0 \end{aligned} \tag{B.4}$$

As highlighted the flux jacobian matrix for the primitive $\tilde{\boldsymbol{A}}$ is then obtained and one can show that the eigenvalues are the same for both formulation with the diagonalisation property of inversible matrices. Let's define the $\boldsymbol{P}$ and $\boldsymbol{Q}$ respectively as the left and right eigenvectors of $\boldsymbol{A}$,

$$\boldsymbol{A} = \boldsymbol{P}\boldsymbol{\Lambda}\boldsymbol{P}^{-1} = \boldsymbol{Q}^{-1}\boldsymbol{\Lambda}\boldsymbol{Q} \tag{B.5}$$

then from the definition of $\tilde{\boldsymbol{A}}$,

$$\tilde{\boldsymbol{A}} = \boldsymbol{M}^{-1}\boldsymbol{A}\boldsymbol{M} = \underbrace{\boldsymbol{M}^{-1}\boldsymbol{P}}_{=\boldsymbol{L}}\boldsymbol{\Lambda}\boldsymbol{P}^{-1}\boldsymbol{M} = \boldsymbol{M}^{-1}\boldsymbol{Q}^{-1}\boldsymbol{\Lambda}\underbrace{\boldsymbol{Q}\boldsymbol{M}}_{=\boldsymbol{R}} \tag{B.6}$$

the eigenvalues matrix remains the same, while the left and right eigenvectors of the primitive jacobian matrix are defined respectively as $\boldsymbol{L} = \boldsymbol{M}^{-1}\boldsymbol{P}$ and $\boldsymbol{R} = \boldsymbol{Q}\boldsymbol{M}$.

The characteristic variables $\boldsymbol{W}$ are then found by injecting the diagonlisation expression of $\tilde{\boldsymbol{A}}$ back in the primitive formulation.

$$\begin{aligned} \partial_t \boldsymbol{V} + \boldsymbol{L}\boldsymbol{\Lambda}\boldsymbol{L}^{-1}\partial_x \boldsymbol{V} &= 0 \\ \underbrace{\boldsymbol{L}^{-1}\partial_t \boldsymbol{V}}_{=\partial_t \boldsymbol{W}} + \boldsymbol{\Lambda}\underbrace{\boldsymbol{L}^{-1}\partial_x \boldsymbol{V}}_{=\partial_x \boldsymbol{W}} &= 0 \end{aligned} \tag{B.7}$$

The characteristic variables are $\partial \boldsymbol{W} = \boldsymbol{L}^{-1}\partial \boldsymbol{V}$, since the eigenvalues matrix is a diagonal the caracteritic curves associated to each W_i corresponds to a 1D wave propagating (in the left or right direction) through the domain at a velocity λ_i. Note that if $\boldsymbol{L}^{-1}$ is constant in time and space then $\boldsymbol{W} = \boldsymbol{L}^{-1}\boldsymbol{V}$.

B.2 Characteristic analysis

In this section, an analysis of the characteristics is done for a given choice of primitive variables. The goal is then to infer the appriopriate choice of variables to impose for different type of boundary conditions. Here only the subsonic inlet and outlet boundary condition are explored as these are relevant in the context of this work, other example are further detailled in [28]. Let's choose the set of primitive variable

$$\boldsymbol{V} = \begin{bmatrix} \rho & u & p \end{bmatrix}^{\mathsf{T}} \tag{B.8}$$

the associated flux jacobian matrix can be shown to be the following.

$$\boldsymbol{A} = \begin{bmatrix} u & \rho & 0 \\ 0 & u & 1/\rho \\ 0 & \rho c^2 & u \end{bmatrix} \tag{B.9}$$

The characteristics of the system are then found following the method detailled in the previous section.

$$\boldsymbol{L}^{-1} = \begin{bmatrix} 0 & 1 & -1/\rho c \\ 1 & 0 & -1/c^2 \\ 0 & 1 & 1/\rho c \end{bmatrix} \quad \Rightarrow \quad \partial \boldsymbol{W} = \boldsymbol{L}^{-1} \partial \boldsymbol{V} \tag{B.10}$$

One can then determine the characteric equations with the left eigenvectors from the diagonalisation property of the jacobian matrix $\boldsymbol{A}$ where $\boldsymbol{\Lambda}$ is the eigenvalues matrix. This in turn gives that in a direction $dx/dt = \lambda_i$, the relation $\boldsymbol{L}_i d\boldsymbol{W} = 0$ is respected. The caracteristic equations associated to each wave speed are then the following.

$$\begin{aligned} dp - \rho c\, du = 0 \quad \text{for} \quad \frac{dx}{dt} = \lambda_0 = u - c \\ dp - c^2\, d\rho = 0 \quad \text{for} \quad \frac{dx}{dt} = \lambda_1 = u \\ dp + \rho c\, du = 0 \quad \text{for} \quad \frac{dx}{dt} = \lambda_2 = u + c \end{aligned} \tag{B.11}$$

The appropriate choice of boundary condition can be determine if proceeding the following way, for a small perturbation δ, the following relation is true

$$\delta \boldsymbol{W} = \boldsymbol{L}^{-1} \delta \boldsymbol{V} \quad \Leftrightarrow \quad \delta \boldsymbol{W} = \begin{bmatrix} \delta \boldsymbol{W}^P \\ \delta \boldsymbol{W}^N \end{bmatrix} = \begin{bmatrix} (\boldsymbol{L}^{-1})^P_I & (\boldsymbol{L}^{-1})^P_{II} \\ (\boldsymbol{L}^{-1})^N_I & (\boldsymbol{L}^{-1})^N_{II} \end{bmatrix} \begin{bmatrix} \delta \boldsymbol{V}^I \\ \delta \boldsymbol{V}^{II} \end{bmatrix} \tag{B.12}$$

where P and N refer to physical and numerical variables, while I and II are the primitive variable determined from inside the domain or from information outside the domain. It can be shown [28] that the solution inside the domain can fully be defined if

$$\det \left(\boldsymbol{L}^{-1} \right)^N_{II} \neq 0 \tag{B.13}$$

or in other words if $(\boldsymbol{L}^{-1})^N_{II}$ is full rank.

Let's then consider the following practical application of a subsonic inlet boundary condition. The ingoing characteristics are λ_1, λ_2 while λ_1 exits the domain. Therefore two characteristic variables need to be imposed. From there, the Eq. (B.12) is reorganised as with the physically imposed characteristic variable on top of the characteristic variable vector. The condition in Eq. (B.13) is then checked for all possible primitive variable combinations. One can then show that the only combination of primitive variable that do not work is to impose the speed and pressure but the density.

$$\left[\begin{array}{c} \delta W_1 \\ \delta W_2 \\ \hline \delta W_0 \end{array}\right] = \left[\begin{array}{cc|c} 1 & 0 & -1/c^2 \\ 0 & 1 & 1/\rho c \\ \hline 0 & 1 & -1/\rho c \end{array}\right] \left[\begin{array}{c} \rho \\ u \\ \hline p \end{array}\right] = \left[\begin{array}{cc|c} 1 & -1/c^2 & 0 \\ 0 & 1/\rho c & 1 \\ \hline 0 & -1/\rho c & 1 \end{array}\right] \left[\begin{array}{c} \rho \\ p \\ \hline u \end{array}\right] = \left[\begin{array}{cc|c} 0 & -1/c^2 & 1 \\ 1 & 1/\rho c & 0 \\ \hline 1 & -1/\rho c & 0 \end{array}\right] \left[\begin{array}{c} u \\ p \\ \hline \rho \end{array}\right]$$

Bibliography

[1] J. C. Adam et al. "Physics, simulation and diagnostics of Hall effect thrusters". In: *Plasma Phys. Control. Fusion* 50, 124041 (2008).

[2] J. Annaloro et al. "Global rate coefficients for ionization and recombination of carbon, nitrogen, oxygen, and argon". In: *Physics of Plasmas* 19 (2012).

[3] F. Bassi and S. Rebay. "Numerical evaluation of two discontinuous Galerkin methods for the compressible Navier–Stokes equations". In: *Int. J. Numer. Meth. Fluids* 40 (2002), pp. 197–207.

[4] A. Bellemans et al. "Reduced-order kinetic plasma models using principal component analysis: Model formulation and manifold sensitivity". In: *Physical Review Fluid* 2 (2017).

[5] M. S. Benilov. "A kinetic derivation of multifluid equations for multispecies nonequilibrium mixtures of reacting gases". In: *Physics of Plasmas* 4 (1997).

[6] M. S. Benilov. "Momentum and energy exchange between species of a multicomponent gas mixture due to inelastic and reactive collisions". In: *Physics of Plasmas* 3, 2805 (1996).

[7] Stefano Boccelli et al. "Lagrangian diffusive reactor for detailed thermochemical computations of plasma flows". In: *Plasma Sources Science and Technology* 28 (2019).

[8] J. Boeuf. "Plasma display panels: physics, recent developments and key issues". In: *J. Phys. D: Appl. Phys.* 36, 6 (2003).

[9] J.-P. Boeuf. "Tutorial: Physics and modeling of Hall thrusters". In: *J. Appl. Phys.* 121 (2017).

[10] C. Boniface et al. "Anomalous cross field electron transport in a Hall effect thruster". In: *Appl. Phys. Lett.* 89, 161503 (2006).

[11] Allen H. Boozer. "Theory of tokamak disruptions". In: *Phys. Plasmas* 19, 058101 (2012).

[12] T. G. Brown. "Three Confinement Systems—Spherical Tokamak, Standard Tokamak, and Stellarator: A Comparison of Key Component Cost Elements". In: *IEEE Transactions on plasma science* 46, 6 (2018).

[13] M. Carrión et al. "Implementation of all-Mach Roe-type schemes in fully implicit CFD solvers – demonstration for wind turbine flows". In: *Int. J. Numer. Meth. Fluids* 73 (2013).

[14] Pascal Chabert. *Physics of Radio-frequency Plasmas*. Cambridge University Press, 2011. ISBN: 9780521763004.

[15] O. Chapurin et al. "Fluid and hybrid simulations of the ionization instabilities in Hall thruster". In: *J. Appl. Phys.* 132, 053301 (2022).

[16] B. Cockburn et al. "Discontinuous Galerkin methods: theory, computation and applications". In: *Springer Science Business Medias* 11 (2012).

[17] N. Corthouts et al. "Travail de Fin d'Etudes : Discontinuous Galerkin Finite Element Method Applied to Plasma Flows". MA thesis. Université de Liège, Liège, Belgique, 2020.

[18] F. Custinne et al. “Master thesis and internship[BR]- Master’s thesis : Plasma sheath modeling with a high order Discontinuous Galerkin Method[BR]- Integration internship”. MA thesis. Université de Liège, Liège, Belgique, 2021.

[19] P. Degond. “Asymptotic-preserving schemes for fluid models of plasmas”. In: *arXiv preprint arXiv:1104.1869* (2011).

[20] E. Deriaz and P. Haldenwang. “Non-linear CFL Conditions Issued from the von Neumann Stability Analysis for the Transport Equation”. In: *Journal of Scientific Computing* 85 (2020).

[21] Eleuterio F. Toro. *Riemann Solvers and Numerical Methods for Fluid Dynamics*. 3rd ed. Springer-Verlag Berlin Heidelberg, 2009.

[22] F. Bassi et al. “High-order accurate p-multigrid discontinuous Galerkin solution of the Euler equations.” In: *Int. J. Numer. Meth. Fluids* 60 (2009), pp. 847–865.

[23] F. Bassi and S. Rebay. “A high-order accurate discontinuous nite element method for the numerical solution of the compressible Navier–Stokes equations.” In: *Journal of Computational Physics* 131 (1997), pp. 267–279.

[24] D. M. Goebel and I. Katz. “Fundamentals of electric propulsion: ion and Hall thrusters”. In: *John Wiley Sons* 1 (2008).

[25] B. Graille, T. E. Magin, and M. Massot. “Kinetic theory of plasmas: Translational energy”. In: *Mathematical Models and Methods in Applied Sciences* 19 (2009), pp. 527–599.

[26] V. Van der Haegen. “Developent of an all-speed approximate Riemann solver applied to supersonic plasmas”. MA thesis. von Karman Institute for Fluid Dynamics, 2013.

[27] Ami Harten. “High Resolution Schemes for Hyperbolic Conservation Laws”. In: *Journal of Computational Physics* 135 (1997), pp. 260–278.

[28] C. Hirsch. *Numerical computation of internal and external flows*. Vol. 2 : Computational Methods for Inviscid and Viscous Flows. John Wiley Sons, 1991.

[29] J. D. Anderson Jr. *Hypersonic and High Temperature Gas Dynamics*. 2nd ed. American Institute of Aeronautics and Astronautics, Inc, 2006.

[30] K. Hillewaert et al. “Hierarchic multigrid iteration strategy for the discontinuous Galerkin solution of the steady Euler equations.” In: *Int. J. Numer. Meth. Fluids* 51 (2006), pp. 1157–1176.

[31] M. G. Kapper and J.-L. Cambier. “Ionizing shocks in argon. Part I: Collisional-radiative model and steady-state structure”. In: *Journal of Applied Physics* 109, 113309 (2011).

[32] M. G. Kapper and J.-L. Cambier. “Ionizing shocks in argon. Part II: Transient and multi-dimensional effects”. In: *Journal of Applied Physics* 109, 113309 (2011).

[33] M. Keidar et al. “Plasma flow and plasma–wall transition in Hall thruster channel”. In: *Physics of Plasmas* 8, 12 (2001).

[34] Hillewaert Koen. “Development of the discontinuous Galerkin method for high-resolution, large scale CFD and acoustics in industrial geometries”. PhD thesis. Université Catholique de Louvain, 2013.

[35] Alejandro Alvarez Laguna. “Multi-Fluid Modeling of Magnetic Reconnection in Solar Partially Ionized and Laboratory Plasmas”. PhD thesis. Katholieke Universiteit Leuven, 2017.

[36] M. Laroussi. “Cold Plasma in Medicine and Healthcare: The New Frontier in Low Temperature Plasma Applications”. In: *Frontiers in Physics* 8 (2020).

[37] Meng-Sing Liou. "A sequel to AUSM, Part II: AUSM+-up for all speeds". In: *Journal of Computational Physics* 214 (2006), pp. 137–170.

[38] Alessandro Munafo. "Multi-Scale Models and Computational Methods for Aerothermodynamics". PhD thesis. École Centrale Paris, 2014.

[39] P. O. Persson and J. Peraire. "Newton-GMRES preconditioning for Discontinuous Galerkin discretizations of the Navier-Stokes equations." In: *Siam J. Sci. Comput.* 30 (2008), pp. 2709–2733.

[40] R. S. Devoto. "Transport coefficients of ionized argon". In: *Physics of Fluids* 16, 616 (1973).

[41] P. L. Roe. "Approximate Riemann Solvers, Parameter Vectors, and Difference Schemes". In: *Journal of Computational Physics* 135 (1997), pp. 250–258.

[42] S. Chapman and T. G. Cowling. *The Mathematical Theory of Non-Uniform Gases: An Account of the Kinetic Theory of Viscosity, Thermal Conduction and Diffusion in Gases*. 2nd ed. Cambridge University Press, 1952.

[43] S. I. Braginskii. "Transport processes in a plasma". In: *Reviews of Plasma Physics* 1 (1965), p. 205.

[44] D. A. Schwer. "An adaptive chemistry approach to modeling complex kinetics in reacting flows". In: *Combustion and Flame* 133 (2003).

[45] M. James B. Scoggins. "Development of numerical methods and study of coupled flow, radiation, and ablation phenomena for atmospheric entry". PhD thesis. Université Paris-Saclay, 2017.

[46] F. C. Tang. "Effects of impurities on shock wave stability and structure in ionizing monoatomic gases". MA thesis. Institute for Aerospace Studies, University of Toronto, 1977.

[47] J. Vlcek. "A collisional-radiative model applicable to argon discharges over a wide range of conditions. I. Formulation and basic data". In: *J. Phys. D: Appl. Phys.* 22 (1989).

[48] Xue-song Li and Chun-wei Gu. "Mechanism of Roe-type schemes for all-speed flows and its application". In: *Computers and Fluids* 86 (2013), pp. 56–70.

[49] V. M. Zhdanov. *Transport Processes in Multicomponent Plasma*. Taylor Francis Group, 2002. ISBN: 0415279208.